Biomedicine & Pharmacotherapy 94 (2017) 499–513

Available online at
ScienceDirect
www.sciencedirect.com

Elsevier Masson France
EM|consulte
www.em-consulte.com/en

Design and synthesis of 2,6-di(substituted phenyl)thiazolo[3,2-b]-1,2,4-triazoles as α-glucosidase and α-amylase inhibitors, co-relative Pharmacokinetics and 3D QSAR and risk analysis

Pervaiz Ali Channar[a], Aamer Saeed[a,*], Fayaz Ali Larik[a,*], Sajid Rashid[b], Qaiser Iqbal[a], Maryam Rozi[b], Saima Younis[b], Jamaluddin Mahar[a]

[a] Department of Chemistry, Quaid-I-Azam University, Islamabad 45320, Pakistan
[b] National Centre for Bioinformatics, Quaid-I-Azam University, Islamabad 45320, Pakistan

ARTICLE INFO

Article history:
Received 28 May 2017
Received in revised form 19 July 2017
Accepted 27 July 2017

Keywords:
Thiazole
Triazolo
Anti-diabetic
α-Glucosidase and α-amylase inhibitors
Butyrylcholinesterase
3D QSAR
Pharmacokinetics
Risk analysis

ABSTRACT

Ten fused heterocyclic derivatives bearing the 2,6-di(subsituted phenyl)thiazolo[3,2-b]-1,2,4-triazoles as central rings were synthesized and structures of the compounds were established by analytical and spectral data using FTIR, EI-MS, ^{1}H NMR and ^{13}C NMR techniques. In vitro inhibitory activities of synthesized compounds on α-amylase, α-glucosidase and α-burylcholinesterase (α-BuChE) were evaluated using a purified enzyme assays. Compound **5c** demonstrated strong and selective α-amylase inhibitory activity (IC_{50} = 1.1 μmol/g). **5 g** exhibited excellent inhibition against α-glucosidase (IC_{50} = 1.2 μmol/g) when compared with acarbose (IC_{50} = 4.7 μmol/g) as a positive reference. Compound 5i was found to be most potent derivative against α-BuChE with the IC_{50} of 1.5 μmol/g which was comparable to the value obtained for (4.7 μmol/g) positive control (i.e. galantamine hydrobromide). Molecular dockings of synthesized compounds into the binding sites of human pancreatic α-amylase, intestinal maltase-glucoamylase and neuronal α-butrylcholinesterase allowed to shed light on the affinity and binding mode of these novel inhibitors. Preliminary structure–activity relationship (SAR) studies were carried out to understand the relationship between molecular structural features and inhibition activities of synthesized derivatives. These data suggested that compounds **5c**, **5 g** and **5i** are promising candidates for hitto- lead follow-up in the drug-discovery process for the treatment of Alzheimer's disease and hyperinsulinamia.

1. Introduction

Heterocyclic compounds are potentially important nuclei for drug discovery as they can interact with diverse molecular targets with wide range of binding interaction possibilities. They are important building blocks in variety of areas, such as many natural products, medicines and functional material [1]. Thiazole and triazole motif bears sulphur and nitrogen atoms in their five membered rings and are key structural units in many pharmaceutical preparations. A scaffold bearing two fused rings of thiazole and triazolo is a condensed heterocyclic compound with one of two isomeric forms naming thiazolo[3,2-b][1,2,4]triazole and thiazolo [2,3-c][1,2,4]triazole. The thiazolo [3,2-b-1,2,4]triazole nucleus is unarguably one of the most significant heterocycles found in numerous natural products and bioactive molecules [2].

Triazole derivatives are the promising heterocycles in the field of medicine. They are the most explored clinical entities both in single and fused forms with other biologically active heterocycles [3]. Most notable isomers are 1*H*-[1,2,4]-triazoles as they form a part of a number of biologically active pharmaceutical products [4]. A large number of [1,2,4]-triazole derivatives exhibit antibacterial [5–8] antifungal [9–11], antitubercular [12–14], analgesic [15–17], anti-inflammatory [18–20], anticancer [21,22], anticonvulsant [23–25], antiviral [26,27], antimalarial [28,29] and other activities.

In this context, thiazole derivatives also have a variety of applications such as bacteriostatics [30–32], antibiotics [33], antifungal [34], CNS regulants of high selling diuretics [35], local anaesthetics [36], anti-inflammatory [37,38], analgesic and anti-pyretics [39,40], HIV infections [41,42], anti-allergic [43], anti-hypertensive [44], against schizophrenia [45], anti-diabetic [46], anthelminthic [47], anticancer [48,49] and antioxidant [50,51].

* Corresponding authors.
E-mail addresses: aamersaeed@yahoo.com (A. Saeed), fayazali@chem.qau.edu.pk (F.A. Larik).

http://dx.doi.org/10.1016/j.biopha.2017.07.139
0753-3322/

Furthermore, the thiazole ring is also found in many potent bioactive molecules. Meloxicam is a new NSAID with a thiazolyl group in its structure. Some other thiazole derivatives such as Niridazole and Ritonavir are antiulcer and antiretroviral agents.

Previously, thiazole and triazole have been reported as potent α-glucosidase inhibitors for controlling blood sugar levels in diabetes mellitus [52]. A series of 1,3-thiazoles have been synthesized and evaluated for their anti-diabetic activity by α-amylase inhibition assay and few triazole compounds exhibited a reversible inhibition of the competitive and non-competitive types for both α-glucosidase and α-amylase [53,54]. Triazole-containing berberine derivatives were inhibitors of both acetylcholinesterase (AChE) and butyrylcholinesterase (α-BuChE) and most of the compounds exhibiting AChE inhibition consisted of heterocyclic ring systems such as 1,2,4-triazole [55–57].

In view of above facts, the fused thiazolo[3,2-b]1,2,4-triazoles are interesting classes of compounds possessing broad spectrum of biological activities, such as antimicrobial [58,59], anticancer [60], anti-inflammatory [61], antipyretic [62] and analgesic as well as antihypertensive actions. However, their inhibition action against human starch digesting enzymes and α-BuChE for the treatment of type II diabetes and Alzheimer's disease has not been investigated yet. Our recent study proved for the first time that thiazolo[3,2-b][1,2,4]-triazoles derivatives demonstrate significant inhibitory action against human pancreatic α-amylase and intestinal α-glucosidase (N-terminal maltase-glucoamylase abbreviated as N-MGAM) and neuronal α-BuChE.

To this extent, several new condensed heterocyclic compounds with phenyl moiety and bridgehead nitrogen from thiazolo [3,2-b] [1,2,4] triazole class were designed and evaluated for their inhibition potential in suppressing hyderglycemia and Alzheimer's disease in present study. Previously reported these type of compounds were exploited for uni target bioevaluation but herein, we have explored the multi-target biological potential of title compounds. Thiazole and triazole are well recognized medicinally active heterocyclic units and this prompted us to design molecules based on these two motifs and seek their multi-target biological potential. Molecular docking studies were performed to define the models for comprehension of binding interactions and to delineate the binding affinity of the molecules in the active sites of target proteins. To a step further, quantitative structure-activity relationship (QSAR) correlated molecular properties with antidiabetic and anticholinesterase activities of the synthesized compounds.

2. Methods and materials

2.1. Chemistry

Commercially available reagents and solvents, purchased from Merck and Sigma Aldrich, were dried and distilled according to standard procedures prior to use. Melting points were determined using a digital Gallenkamp (SANYO) model MPD.BM 3.5 apparatus and are uncorrected. FTIR spectra were recorded with tetramethylsilane as internal standard using Bio-Rad-Excalibur Series Mode FTS 3000 MX spectrophotometer. NMR spectra were obtained with AVANCE AV 300 MHZ spectrometers using DMSO and acetone as solvent for accurate NMR analysis. TMS was used as internal standard. The Finnegan MAT-311A spectrometer was used for electron impact mass spectra (EI-MS) analysis. An internal standard cesium iodide (CsI) was used for mass measurement. Column chromatography was performed using silica gel (E. Merck, type 60, 70–230 mesh). Pre-coated silica gel aluminum plates (Kieselgel 60, 20 × 20 and 0.5 mm thick, E. Merck, Germany) were used for TLC analysis. Light of wavelength 254 and 365 nm were used to visualize the chromatogram.

2.2. Procedure for synthesis of thiazolo [3,2-b] [1,2,4] triazoles (5a-5j)

The aryl thiazole [3,2-b] [1,2,4] triazoles were synthesized by refluxing 0.001 mol of the respective ethanone in 4 ml of phosphorous oxychloride. The products were purified by recrystallization from ethanol, column chromatography or TLC. The structures of all compounds were established through EI-MS and HNMR. Spectral data of the synthesized compounds are described below.

6-(4-bromophenyl)-2-(3-chlorophenyl) thiazolo [3,2-b] [1,2,4]triazole (5a)

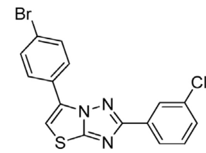

white crystalline solid; yield; 60%; m.p: 225–228 °C; Rf; 0.69 (*n*-hexane:ethylacetate, 8:2); **FTIR** (neat, cm^{-1}); 3094 (C_{sp2}-H), 1425 (C=N), 1578 (C=C), 1501 (C=C); **^{1}H NMR** (300 MHz, DMSO): δ 8.10-8.12 (m, 1H, Ar-H), 7.90-8.04 (m, 1H, Ar-H), 7.93-7.96 (m,1H, Ar-H), 7.56-7.63 (m, 3H, Ar-H), 7.26-7.34 (m, 2H, Ar-H); 6.9 (s, 1H) **^{13}C NMR** (75 MHz, DMSO): δ 161.57, 139.52, 136.97, 133.16, 131.64, 131.28, 129.42, 129.34, 129.33, 128.84, 126.34, 122.76, 120.96, 118 **Anal.** Calcd. For $C_{16}H_9BrClN_3S$: C, 49.19, H, 2.32, N, 10.76, S, 8.21 found: C, 50.48, H, 3.1, N, 11.8, S, 9.1. Found: 388.94

2-(4-nitrophenyl)-6-(m-tolyl) thiazolo [3,2-b] [1,2,4]triazole (5b)

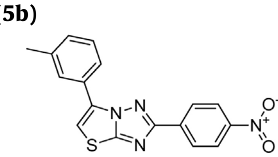

yellow crystalline solid; yield; 70%; m.p: 235–238 °C; Rf; 0.51 (*n*-hexane: ethylacetate, 8:2); **FTIR** (neat, cm^{-1}); 3084 (C_{sp2}—H), 1435 (C=N), 1570 (C=C), 1520 (C=C); **^{1}H NMR** (300 MHz, DMSO): δ 8.10-8.12 (m, 1H, Ar-H), 7.90-8.04 (m, 1H, Ar-H), 7.93-7.96 (m,1H, Ar-H), 7.56-7.63 (m, 3H, Ar-H), 7.26-7.34 (m, 2H, Ar-H), 6.8 (s,1H),2.34 (s, 3H, CH_3); **^{13}C NMR** (75 MHz, DMSO): δ 161.57, 139.52, 136.97, 133.16, 131.64, 131.28, 129.42, 129.34, 129.33, 128.84, 126.34, 122.76, 120.96, 119, 30 **Anal.** Calcd. For $C_{17}H_{12}N_4O_2S$: C, 60.70, H, 3.60, N, 16.66, S, 9.53 found: C, 61.48, H, 3.9, N, 17.8, S, 10.2 Found: 336.07

6-(3-nitrophenyl)-2-(m-tolyl) thiazolo [3,2-b] [1,2,4]triazole (5c)

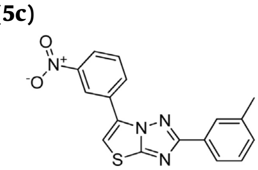

brown crystalline solid; yield; 75%; m.p: 240 °C; Rf; 0.54 (*n*-hexane: ethylacetate, 8:2); **FTIR** (neat, cm^{-1}); 3073 (C_{sp2}-H), 1430 (C=N), 1575 (C=C), 1525 (C=C); **^{1}H NMR** (300 MHz, DMSO): δ 8.12-8.15 (m, 1H, Ar-H), 7.80-8.08 (m, 1H, Ar-H), 7.93-7.96 (m,1H, Ar-H), 7.56-7.63 (m, 3H, Ar-H), 7.26-7.34 (m, 2H, Ar-H), 6.6 (s,1H), 2.37 (s, 3H, CH_3); **^{13}C NMR** (75 MHz, DMSO): δ 164.57, 140.52, 134.97, 133.18, 131.84, 131.28, 129.42, 129.34, 129.33, 128.84, 126.34, 122.76, 120.96, 119, 28 **Anal.** Calcd. For $C_{17}H_{12}N_4O_2S$: C, 60.70, H, 3.60, N, 16.66, S, 9.53 found: C, 61.48, H, 3.9, N, 17.8, S, 10.2 found: 336.07

6-(4-chlorophenyl)-2-(4-fluorophenyl) thiazolo [3,2-b] [1,2,4]triazole (5d)

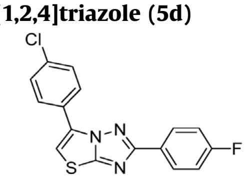

pink crystalline solid; yield; 78%; m.p: 243 °C; Rf; 0.44 (*n*-hexane: ethylacetate, 8:2); **FTIR** (neat, cm^{-1}); 3077 (C_{sp2}—H), 1433 (C=N), 1573 (C=C), 1528 (C=C); **^{1}H NMR**

(300 MHz, DMSO): δ 8.15 (s, 1H, SCH), 8.14-8.18 (m, 1H, Ar-H), 7.70-8.08 (m, 1H, Ar-H), 7.90-7.98 (m,1H, Ar-H), 7.52-7.65 (m, 3H, Ar-H), 7.23-7.34 (m, 2H, Ar-H) 6.7 (s,1H); **^{13}C NMR** (75 MHz, DMSO): δ 168.57, 142.52, 136.97, 134.18, 131.84, 131.28, 129.42, 129.34, 129.33, 128.84, 126.34, 122.76, 120.96, 119. **Anal.** Calcd. For $C_{16}H_9ClFN_3S$: C, 58.27, H, 2.70, N, 12.74, S, 9.73 found: C, 59.48, H, 2.9, N, 12.8, S, 9.9 found: 329.07

6-(4-chlorophenyl)-2-(3, 4, 5-trimethoxyphenyl) thiazolo [3,2-b] [1,2,4]triazole (5e)

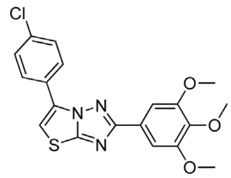

yellow crystalline solid; yield; 88%; m.p: 247 °C; Rf; 0.74 (*n*-hexane: ethylacetate, 8:2); **FTIR** (neat, cm^{-1}); 3079 (C_{sp2}—H), 1445 (C=N), 1579 (C=C), 1538 (C=C); **^{1}H NMR** (300 MHz, DMSO): δ 8.44-8.58 (m, 1H, Ar-H), 7.70-8.08 (m, 1H, Ar-H), 7.90-7.98 (m,1H, Ar-H), 7.52-7.65 (m, 3H, Ar-H), 7.23-7.34 (m, 2H, Ar-H),6.5 (s, 1H), 3.33 (s, 9H, CH_3); **^{13}C NMR** (75 MHz, DMSO): δ 168.57, 142.52, 136.97, 134.18, 131.84, 131.28, 129.42, 129.34, 129.33, 128.84, 126.34, 122.76, 120.96, 119, 55. **Anal.** Calcd. For $C_{19}H_{16}ClN_3O_3S$: C, 58.27, H, 2.70, N, 12.74, S, 9.73 found: C, 59.48, H, 2.9, N, 12.8, S, 9.9 found: 329.07

6-(4-bromophenyl)-2-(3-fluorophenyl) thiazolo [3,2-b] [1,2,4]triazole (5f)

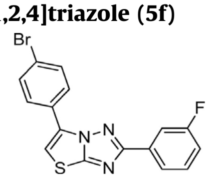

yellow crystalline solid; yield; 81%; m.p: 229 °C; Rf; 0.54 (*n*-hexane: ethylacetate, 8:2); **FTIR** (neat, cm^{-1}); 3066 (C_{sp2}—H), 1434 (C=N), 1563 (C=C), 1522 (C=C); **^{1}H NMR** (300 MHz, DMSO): δ 8.25-8.39 (m, 1H, Ar-H), 7.70-8.08 (m, 1H, Ar-H), 7.92-7.98 (m,1H, Ar-H), 7.55-7.69 (m, 3H, Ar-H), 7.25-7.38 (m, 2H, Ar-H) 6.5 (s, 1H);**^{13}C NMR** (75 MHz, DMSO): δ 168.57, 142.52, 136.97, 134.18, 131.84, 131.28, 129.42, 129.34, 129.33, 128.84, 126.34, 122.76, 120.96, 119. **Anal.** Calcd. For $C_{16}H_9BrFN_3S$: C, 51.27, H, 2.42, N, 11.23, S, 8.57 found: C, 51.35, H, 2.4, N, 11.23, S, 8.57 found: 374.97

6-(3-bromophenyl)-2-(4-chlorophenyl) thiazolo [3,2-b] [1,2,4] triazole (5 g)

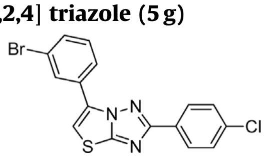

yellow crystalline solid; yield; 88%; m.p: 232 °C; Rf; 0.46 (*n*-hexane: ethylacetate, 8:2); **FTIR** (neat, cm^{-1}); 3073 (C_{sp2}—H), 1439 (C=N), 1573 (C=C), 1528 (C=C); **^{1}H NMR** (300 MHz, DMSO): δ 8.14-8.18 (m, 1H, Ar-H), 7.70-8.08 (m, 1H, Ar-H), 7.90-7.98 (m,1H, Ar-H), 7.52-7.65 (m, 3H, Ar-H), 7.23-7.34 (m, 2H, Ar-H),6.8(s, 1H); **^{13}C NMR** (75 MHz, DMSO): δ 166.57, 141.52, 137.97, 135.18, 132.84, 130.28, 128.42, 127.34, 126.33, 125.84, 123.34, 122.76, 120.96, 119. **Anal.** Calcd. For $C_{16}H_9BrClN_3S$: C, 49.19, H, 2.32, N, 10.23, S, 8.21 found: C, 49.35, H, 2.34, N, 10.76, S, 8.21 found: 390.97

6-(3-bromophenyl)-2-(3, 4-dimethylphenyl) thiazolo [3,2-b] [1,2,4] triazole (5 h)

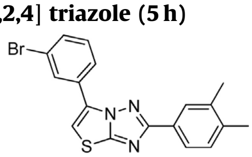

white crystalline solid; yield; 84%; m.p: 247 °C; Rf; 0.54 (*n*-hexane: ethylacetate, 8:2); **FTIR** (neat, cm^{-1}); 3073 (C_{sp2}—H), 1439 (C=N), 1573 (C=C), 1528 (C=C); **^{1}H NMR** (300 MHz, DMSO): δ 8.24-8.38 (m, 1H, Ar-H), 7.70-8.08 (m, 1H, Ar-H), 7.92-7.98 (m,1H, Ar-H), 7.55-7.69 (m, 3H, Ar-H), 7.25-7.38 (m, 2H, Ar-H); 6.9 (s, 1H), 2.32 (s, 3H);**^{13}C NMR** (75 MHz, DMSO): δ 168.57, 142.52, 136.97, 134.18, 131.84, 131.28, 129.42, 129.34, 129.33, 128.84, 126.34, 122.76, 120.96, 119,29. **Anal.** Calcd. For $C_{18}H_{14}BrN_3S$: C, 56.27, H, 3.67, N, 10.93, S, 8.34 found: C, 57.35, H, 3.4, N, 11.23, S, 8.57 found: 384.29

6-(4-chlorophenyl)-2-(4-methoxy-3-methylphenyl) thiazolo [3,2-b] [1,2,4]triazole (5i)

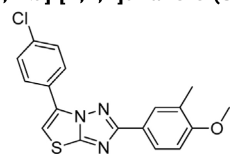

white crystalline solid; yield; 78%; m.p: 220 °C; Rf; 0.74 (*n*-hexane: ethylacetate, 8:2); **FTIR** (neat, cm^{-1}); 3073 (C_{sp2}—H), 1439 (C=N), 1573 (C=C), 1528 (C=C); **^{1}H NMR** (300 MHz, DMSO): δ 8.25-8.49 (m, 1H, Ar-H), 7.74-8.12 (m, 1H, Ar-H), 7.92-7.98 (m,1H, Ar-H), 7.55-7.69 (m, 3H, Ar-H), 7.25-7.38 (m, 2H, Ar-H); 6.9 (s, 1H),3.4 (s,3H), 2.32 (s, 3H);**^{13}C NMR** (75 MHz, DMSO): δ 164.57, 144.52, 137.97, 135.18, 132.84, 130.28, 129.34, 129.33, 128.84, 126.34, 122.76, 120.96, 119,53,29. **Anal.** Calcd. For $C_{18}H_{14}ClN_3OS$: C, 60.76, H, 3.97, N, 11.81, S, 9.01 found: C, 61.35, H, 3.79, N, 11.81, S, 9.01 found: 355.29

2-phenyl-6-(3, 4, 5-trimethoxyphenyl) thiazolo [3,2-b] [1,2,4]triazole (5j)

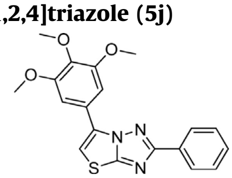

white crystalline solid; yield; 74%; m.p: 210 °C; Rf; 0.64 (*n*-hexane: ethylacetate, 8:2); **FTIR** (neat, cm^{-1}); 3078 (C_{sp2}—H), 1447 (C=N), 1578 (C=C), 1538 (C=C); **^{1}H NMR** (300 MHz, DMSO): δ 8.35-8.49 (m, 1H, Ar-H), 7.74-8.12 (m, 1H, Ar-H), 7.92-7.98 (m,1H, Ar-H), 7.55-7.69 (m, 3H, Ar-H), 7.25-7.38 (m, 2H, Ar-H); 6.9 (s, 1H),3.4 (s,9H);**^{13}C NMR** (75 MHz, DMSO): δ 164.57, 144.52, 137.97, 135.18, 132.84, 130.28, 129.34, 129.33, 128.84, 126.34, 122.76, 120.96, 119,53,29. **Anal.** Calcd. For $C_{19}H_{17}N_3O_3S$: C, 62.27, H, 4.67, N, 11.44, S, 8.73 found: C, 62.35, H, 4.8, N, 11.57, S, 8.57 found: 367.10

2.3. Biological assays

2.3.1. α-Amylase assay

The compounds were tested for their enzyme inhibition activity against α-amylase by the previously reported method. For assay 5 μl of the extract with the final concentration of 200, 100 and 50 μg/ml was mixed with 40 μl of starch (0.05%) and 30 μl of potassium phosphate buffer (pH 6.8) in 96-well micro titer plate followed by the addition of 10 μl of α-amylase enzyme (0.2 U/well). Standard drug Acarbose and DMSO were used as positive and negative controls respectively. The plates were incubated for 30 min at 50 °C and 20 μl HCl (1 M) as stopping reagent was added. Then100 μl of iodine reagent (5 mM KI and 5 mM I_2) was added to check the presence and absence of starch and absorbance was measured at 540 nm with microplate reader (Bio Tek, Elx800). The experiments were performed in triplicate and IC_{50} was calculated with Graph pad Prism 5.

2.3.2. Butyrylcholinesterase assay

Ellman's method was used to determine the enzyme inhibition potential of compounds against butyryl cholinestrase (BuChE) [31]. In experiment butyrylthiocholine iodide (BuChI) was used as substrates and assay was performed in triplicate in 96-well plates. The compound (5 μl) with final concentration of 200, 100 and 50 μg/ml was mixed with 20 μl of 100 μM sodium phosphate buffer (pH 8.0) and 5 μl BuChE enzyme (0.05U/ml). Then 10 μl BuChI (4 mM) and 60 μl DTNB (3 mM) was added. Galantamine hydrobromide (Sigma) and DMSO served as a positive and negative control respectively. The reaction mixtures were then incubated for 30 min at 37 °C. After incubation absorbance was measured at 405 nm using a microplate reader (Bio Tek Elx-800, USA) and IC_{50} values were recorded using Graph pad Prism 5.

2.3.3. α-Glucosidase assay

α-Glucosidase enzyme inhibition assay was performed according to the previously reported method. For experiment 25 μl *p*-nitrophenyl-α-D-glucopyranoside, 65 μl phosphate buffer (pH 6.8) and 5 μl α-glucosidase enzyme (0.05U/mL) were mixed in 96-well microtiter plate. 5 μl compound with final concentration 500, 250 and 125 μg/ml was added in respective wells. Acarbose and DMSO were used as positive and negative controls respectively. Plates were incubated at 37 °C for 30 min, followed by the addition of 0.5 mM sodium bicarbonate (100 μl) as stopping agent. Absorbance was measured at 405 nm using microplate reader (BioTek Elx-800, USA) and IC_{50} values were calculated using Graph pad Prism 5.

2.4. Molecular docking studies

The X-ray crystal structures of human maltase-glucoamylase (MGAM) for N-terminal domain (PDB code: 3L4Z), human α-BuChE (PDB ID: 1P0I) and α-amylase (PDB code: 1B2Y) were downloaded from Protein Data Bank and processed subsequently prior to docking. All the water molecules were removed whereas kollman charges, missing residues and essential polar hydrogen atoms were added by the AutoDock tools (Ver 4.2) [63]. Two dimensional structures of synthesized compounds, acarbose (Chembl ID: 1566) and galantamine hydrobromide (Chembl ID: 659) were sketched in ChemDraw [64] and followed by geometry minimization in LigandScout [65]. Mol files of compounds were converted to PDB coordinate files using OpenBabel [66].

Grid box of 66 * 52 * 82 points was used for α-amylase with a spacing 1.0 Å and the grid box center was put on x = −1.617, y = −10.665, and z = −28.351. α-BuChE was enclosed in a 70 * 64 * 74 grid box having 1.0°A spacing and 137.90, 122.76 and 38.68 as x, and y and z centres. A grid map of 68* 58 * 62 points in x, y, and z directions were centered on the NMGAM with a spacing of 1.0°A.

The Lamarckian genetic algorithm (LGA) was applied with the following parameters: initial population of 100 randomly placed individuals, a maximum number of 27,000 generations, a mutation rate of 0.02, 2.5 × 106 energy evaluations and a cross over rate of 0.80, while remaining docking parameters were set to default. The ligands were allowed to move within the target proteins to achieve the lowest energy conformations and the number of runs for each docking procedure was set to 100. Dockings of all the synthesized compounds and control drugs (Acarbose and galantamine hydribromide) with α-amylase, α-BuChE and NMGAM were performed in AutoDock Vina 1.5.6 and most energetically favored orientations were selected for subsequent analysis. Best docked poses in each docking experiment were subjected to LigPlot analysis to visualize receptor-ligand hydrophobic contacts and hydrogen bonded interactions [67].

2.5. QSAR model generation

2.5.1. Molecular structural parameters selection

The compounds in our study were classified in decoy and active datasets based on their strong to weak inhibitory potential against α-amylase, α-BuChE and α-glucosidase. Later on, their diverse molecular properties were assessed to build a preliminary QSAR models. 2D and 3D structural and physiochemical descriptors that describe electronic and steric properties of compounds were retrieved through online interfaces of ChemAxon's Chemicalize [68], Swiss ADME [69] and Molinspiration [70]. Furthermore, optimized molecular structures were imported into standalone Padel-descriptor software and 1445 diverse descriptors (spatial, constitutional, geometrical, electronic, topological counts of chemical substructures and electrotopological state etc.) for each molecule were calculated [71].

2.5.2. Model development and validation

Collected variables with larger values of negative or positive correlation (greater than 0.70 and smaller than −0.50) were considered and methods such as forward selection, backward elimination and stepwise selection were performed to screen the significant molecular descriptors, as done in our previous study (Tegginamath et al., 2011). Subsequent to exclusion of non-significant parameters, multiple regression analysis in IBM statistical package for social sciences (SPSS) version 22 was used to create regression models for predicting inhibition activity against α-amylase, α-BuChE and mammalian α-glucosidase. Cross validation for each model was carried out by inputting descriptor values of the compounds in respective QSAR equations and by comparing expected IC_{50} values from QSAR model with those obtained from the experimental essays [72].

2.6. Pharmacokinetics properties and ADMET analysis

Most of the drugs in discovery process fail to cross clinical trials because of poor Pharmacokinetics (PK). PK determines human therapeutic use of compounds and depends to absorption, distribution, metabolism, excretion, and toxicity (ADMET) properties of compounds under consideration [73,74]. These properties correlate well with pharmacokinetic properties such as molecular weight, TPSA, permeability, octanol-water coefficient (logP) etc. Likewise, 90% of orally active compounds follows Lipinski's rule of five [75]. These ADMET (Absorption, Distribution, Metabolism, Excretion and Toxicity) were predicted through Toxicity checker and Lazar toxicity server to hypothetically measure the positive and negative biological effects of compounds [76,77]. Toxicity parameters such as mutagenic and tumorigenic effects along with drug-likeness values were evaluated through OSIRIS Data Warrior and Chem Axon's Chemicalize which were then later cross checked for compliance with their standard ranges [78,79].

To access the lipophilicity of predicted hits, cLogP (activity/size) values were predicted using ORSIS Data Warrior and compared with pIC_{50} values. Ligand efficiency (LE) and lipophilic efficiency (LipE or LLE) profiles of inhibitors were used to identify the hits with higher activities using Equation 1 and 2 [80,81]. Ligand efficiency indices give an indication of the binding energy per heavy atom and better identify potential drug candidates.

$$LE = \left(\frac{1.37}{HA}\right) * pIC50 \quad (1)$$

$$LipE = pIC50 - clogP \quad (2)$$

Due to variability in heavy atom counts of the ligands, LE values were subsequently scaled as described by [83] to retrieve size-independent ligand efficiency values (LEScale). This was achieved by fitting the top LE values versus heavy atom counts to a simple exponential function (Eq. (3)), as outlined by [82]. Subsequently, "Fit Quality" or "FQ" scoring function (Eq. (4)) was computed to detect the optimal ligand binding properties of synthesized compounds through the ratio of LE and LEScale.

$$LEScale = 0.104 + 0.65e^{-0.037*HA} \quad (3)$$

$$FQ = LE/LEScale \quad (4)$$

3. Results and discussion

3.1. Synthesis of compounds

The synthesis of two heterocycles fused together attached with aromatic rings was carried by using Fischer esterification reaction as the starting conversion from carboxylic acids into corresponding esters and followed by routine transformations for the 5-exo-trig cyclization $POCl_3$ was the reagent selected [33]. Compounds were synthesized in good to better yields (Fig. 1) and the yield of each step is included in Table 1.

Compound 5a bears two different halogen atoms on different phenyl rings and was obtained in minimum yield of 60% compared to other derivatives. Compound 5e was obtained in excellent yield of 88% and this was maximum yield compared to any other compound. Overall, this is a multistep synthetic route and all the steps involved in this synthetic outline are clean and high yielding. Products showed single spot on the TLC plates and there was no any prerequisite of using column chromatography to separate the products.

The compounds were fully characterized by physical techniques. The synthesis of new triazole fused thiazoles was indicated in the FTIR spectra by the presence of two strong peaks between 3078 cm^{-1} that was assigned to sp^2 C—H and 1560 cm^{-1}(indicating presence of aromatic ring) and the absorption bands for C=N appeared at 1470 cm^{-1}. The synthesis of compounds was further confirmed by ^1H NMR spectra. The protons in the vicinity of electron withdrawing groups (NO_2, F) appeared more deshielded (8.4 ppm) compared to the electron donating groups (7.5 ppm) (OMe, Me). In the aromatic part of the spectrum multiplet were observed for monosubstituted rings and doublets of doublets were observed for *para*-substituted rings. The methyl groups appeared at 2.34 ppm which is consistent with their environment being directly attached with aromatic ring. The ^{13}C NMR spectra demonstrated that ipso carbons were found relatively deshielded and the same electronic effect was observed for carbons attached with electron donating or electron withdrawing groups. The downfield absorption of O—CH_3 carbon relative to methyl carbon can be attributed to electronegativity effect exerted by oxygen atom in the case of the latter.

Table 1
Yield of each step.

Compound	Step	Yield
2a-e	1st	97%
3a-e	2nd	92%
4a-e	3rd	91%
5a-e	4th	90%
Ethanones	5th	89%
5a-j	6th	88–60%

3.2. Biological activities

The synthesized compounds were subjected to three different activities. All the compounds showed great inhibition against three enzymes and α-amylase, α-glucosidase and BuChE. In case of α-amylase, selected compounds exhibited higher inhibition potential than acarbose. Particularly, compound **5c** was the most active compound in the series due to presence of nitro group at the meta position which enhanced charge separation by pulling electron density from the ring (Fig. 2). Moreover, its methyl group at meta position resulted in the donation of electron density through no-bond resonance. The compounds showed significant inhibition against α-glucosidase enzyme, and derivative **5g** was found to be the most potent compound in the series due to possession of halogen atoms at aryl rings (Fig. 2). **5g** contains bromine atom at meta position and chlorine atom at the para position. However, few derivatives were found potent against butyrylcholinesterase enzyme and compound **5i** showed better results in the series (Fig. 2). **5i** contained chloro group at the para position of one aryl ring and the other aryl ring was substituted

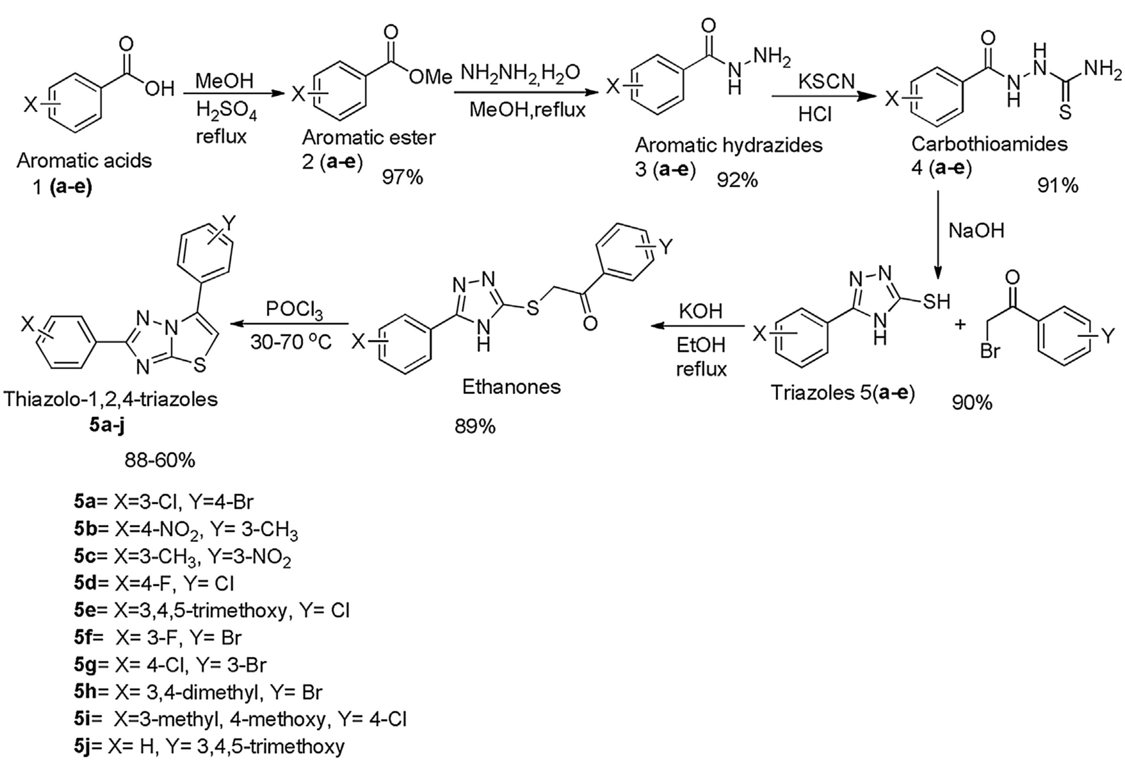

Fig. 1. Synthetic route to 6-Phenyl substituted thiazolo [3,2-b-1,2,4]-triazoles (5a-5j).

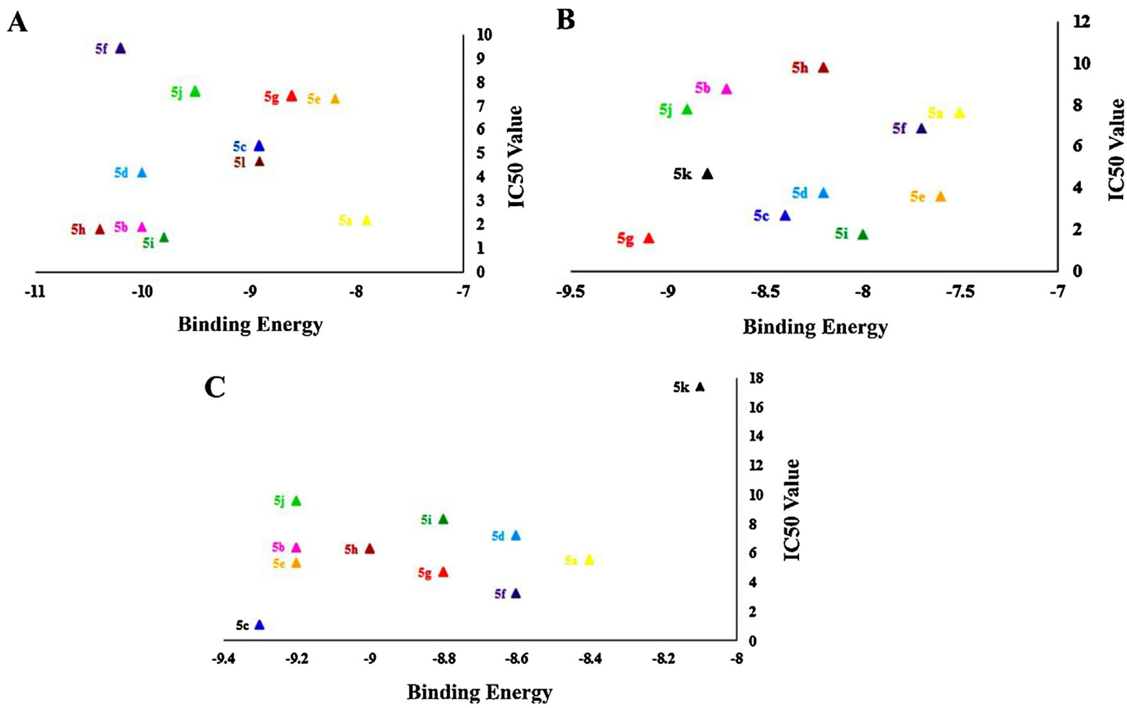

Fig. 2. Binding energy scores of docked complexes vs IC_{50} values of compounds from inhibition essays. A) BuChE, B) maltase-glucoamylase and C) α-amylase. Synthesized compounds are indicated in triangular data labels in following colors: **5a**, Yellow; **5b**, Magenta; **5c**, Dark blue; **5d**, Light blue; **5e**, Orange; **5f**, Purple; **5 g**, Red; **5 h**, Firebrick; **5i**, Dark Green and **5j**, Light green. (For interpretation of the references to colour in this figure legend, the reader is referred to the web version of this article.).

with methoxy and methyl group. Inhibitory activities of synthesized compounds for α-glucosidase, butrylcholinesterase and α-amylase are presented in Table 2.

3.3. Molecular docking analysis

Comparative docking analysis of minimized protein structures were performed with human α-amylase, α-BuChE and human α-glucosidase (N-terminal intestinal maltase-glucoamylase). Each ligand-receptor complex was subjected to careful analysis for ideal docked poses on the basis of least binding energy scores and maximum number of cluster conformations. Binding energy values of stable docked conformations were shown in Table 3. Positioning of ligands onto the surface of α-amylase, α-BuChE and maltase-glucoamylase were keenly monitored to explore the binding pocket dynamics and residual contributions of each protein in association with docked ligand. The detailed residual contributions of individual complexes were shown in Table 3. Generally, structural insights of inhibitor binding to α-amylase, α-BuChE and α-glucosidase revealed predominant contributions of hydrophobic residues lying in the periphery of active sites.

Table 2
Concentrations of the synthesized chemical derivatives for effectively inhibiting α-Amylase, Butrylcholinesterase and α- Glucosidase are given as IC_{50} values. These scores are received from biological assays described in Section 2.3.

Compounds	α-Amylase IC_{50} (μM)	Butrylcholinesterase IC_{50} (μM)	α- Glucosidase IC_{50} (μM)
5a	5.5	2.2	7.6
5b	6.4	1.9	8.8
5c	1.1	5.3	2.7
5d	7.2	4.2	3.8
5e	5.3	7.3	3.6
5f	3.2	9.4	6.9
5g	4.7	7.4	1.6
5h	6.3	1.8	9.8
5i	8.3	1.5	1.8
5j	9.6	7.6	7.8
Acarbose	17.4	–	4.7
Galantamine Bromide	–	4.7	–

3.3.1. Molecular docking study on α-amylase

All the thiazolo[3,2-b]-1,2,4-triazole derivatives clustered inside the active site in a deep depression near the center of α-amylase (Fig. 3). Side chains of Asp165, Asp197, Lys200, Glu233, Asp300 and a number of aromatic or non-polar residues including Trp58, Trp59, Tyr62, His101, Pro163, Ile235, His299 and His305 residues were actively engaged in association with tested compounds as indicated in Fig. 3 [83,84].

Strong inhibitory activity of human α-amylase relies on the formation of hydrogen bonds between the hydroxyl (OH) groups of individual ligand and carboxylic acid side chains of binding cleft residues (Asp197, Glu233 and Asp300). Moreover, the conjugated π-system between Trp59 and Tyr62 indoles and heterocyclic rings of ligands also contributes in binding, as described elsewhere [85,86]. 9 out of 10 ligands constituted efficient π-π interactions with the aromatic side chains of Trp59 and Tyr62, while hydrophobic interactions with the binding site residues (Asp197, Glu233 and Asp300) were noticed in 8, 6 and 7 complexes, respectively (Table). These data indicated the strong inhibitory potential of compounds in current study.

Involvement of hydrogen bonding with the residues of catalytic center (i.e with Gln63 and Asp305 respectively) was witnessed in case of **5c** and **5j**. Paramount significance of Gln63 in the inhibition mechanism was evident by its prominent contribution in making hydrophobic contacts with all the least energy scoring compounds (**5b**, **5e**, **5 h** and **5j**). Furthermore, hydrogen bonding between Gln63 and **5c** may be responsible for lowest IC_{50} value (1.5 μmol/g) in α-amylase inhibition assay.

Table 3
Binding energy profiles of α-amylase, α-BuChE and α-glucosidase with **5a-5j** inhibitors. H-bonded residues are indicated in bold.

Ligands	α-amylase		α-BuChE		Maltase-glycoamylase	
	Binding Energy (kcal/mol)	Binding residues	Binding Energy (kcal/mol)	Binding residues	Binding Energy (kcal/mol)	Binding residues
5a	−8.4	Leu162, Thr163, Asp197, Ala198, Lys200, His201, Glu233, Ile235	−7.9	Phe227, Asn228, Pro303, Asp304, Glu404, Trp522, Thr523	−7.5	Asn212, Leu213, Tyr214, Glu446, Ser448, Lys480, His497, Asn498
5b	−9.2	Trp58, Trp59, Tyr62, Gln63, Gly104, Val107, Asp197, Asp300	−10.0	Asp70, Trp82, Gly115, Gly116, Glu197, Pro285, Ala328, Phe329, Tyr332, Met437, His438, Gly439, Tyr440	−8.7	Asn212, Leu213, Tyr214, Gly215, Ala216, Met241, Glu446, Ser448, Leu477, Lys480, His497, Asn498
5c	−9.3	Trp59, Tyr62, **Gln63,** Tyr151, Leu162, Asp197, His201, Glu233, Ile235, His305	−8.9	Asp70, Trp82, Gly115, Tyr128, Glu197, Pro285, Ala328, Phe329, Tyr332, Trp430	−8.4	Asn212, Leu213, Gly215, Ala216, Ala240, Met241, Glu446, Ile472, Leu477, Lys480, His497, Asn498
5d	−8.6	Trp58, Trp59, Tyr62, Leu162, Asp197, His201, Glu233, Ile235, His299, Asp300, His305	−10.0	Trp82, Gly116, Gly117, Glu197, Ser198, Trp231, Leu286, Ala328, Phe329, Phe398, His438	−8.2	Asn212, Leu213, Tyr214, Gly215, Glu446, Ile472, Leu477, His497, Asn498
5e	−9.2	Trp59, Tyr62, Gln63, Tyr151, Leu162, Leu165, Glu233, Ile235, His305	−8.2	Asn228, Pro230, Asp304, Leu307, Glu308, Tyr396, Cys400, Pro401, Glu404, Trp522, Thr523, Phe526, Pr0527	−7.6	Asn207, Leu213, Tyr214, Gly215, His538, Leu540, Trp552, Glu559, Phe560, Phe563
5f	−8.6	Trp58, Trp59, Tyr62, Leu162, Asp197, His201, Glu233, Ile235, His299, Asp300, His305,	−10.2	Asp70, Trp82, Gly115, Gly116, Tyr128, Glu197, Pro285, Ala328, Phe329, Tyr332	−7.7	Asn212, Leu213, Gly215, Met241, Glu446, Ile472, Leu477, Lys480, His497, Asn498
5g	−8.8	Trp58, Trp59, Tyr62, Gln63, Gly104, Thr163, Leu165, Asp300, His305	−8.6	Asn228, Tyr396, Cys400, Pro401, Glu404, Trp522, Thr523, Phe526, Pro527	−9.1	Asn212, Gly215, Ala216, Ala240, Met241, Ile472, Leu473, Leu477, Cys479, His497, Asn498
5h	−9.0	Trp58, Trp59, Tyr62, Gln63, His101, Gly104, Thr163, Leu165, Asp197, Asp300, His305	−10.4	Asp70, Trp82, Gly115, Tyr128, Glu197, Pro285, Ala328, Phe329, Tyr332, His438	−8.2	Asn207, Leu213, Tyr214, Gly215, His538, Leu540, Trp552, Phe560
5i	−8.8	Trp59, Tyr62, Tyr151, leu162, Asp197, Lys200, Ile235, Asp300	−9.8	Asp70, Trp82, Glu197, Pro285, Ala328, Phe329, Tyr332, Met437, His438, Gly439	−8.0	Asn207, Leu213, Tyr214, Gly215, Gln217, His538, Leu540, Trp552, Phe560
5j	−9.2	Trp59, Tyr62, Gln63, Leu162, Asp197, His201, Ile235, Glu233, His305	−9.5	Asp70, Trp82, Gly115, Tyr128, Glu197, Pro285, Ala328, Phe329, Tyr332, His438	−8.9	Leu213, Tyr214, Gly215, His538, Leu540, Asn543, Asp549, Trp552, Ser553, Glu559, Phe560

Addition of further —OH groups to the structural framework of 5c appears as a promising method to increase the number of hydrogen bonded contacts with catalytic site residues and an overall improvement of IC_{50} value.

3.3.2. Molecular docking study for BuChE

In total, 7 least energy scoring triazole derivatives were accommodated in the active gorge of BuChE, lined by aromatic residues Tyr332, Ala328, Trp82, Tyr128, Gly116, Phe329, Gly115 and Pro285, featuring acidic residue Asp70 at the entrance and Glu197 located at the bottom of gorge (Fig. 3). Potency of 3 hits (**5b**, **5d** and **5 h**) was confirmed by both lower IC_{50} values and least docking scores. Exyanaion hole residues (Gly116, Gly117 and Ala199) stabilize the transition state of bound enzyme and absence of interactions with these residues resulted in slightly higher binding energy score for **5i**. On contrary, interaction with highly conserved N—H dipole derived from the side chain of Gly116 with 5f is accountable for excellent energy score of −10.2 kcal/mol. Three poorly scored ligands (**5a**, **5e** and **5 g**) were surrounded by Asn228, Glu404, Trp522 and Thr523 residues and gathered inside a different pocket in the immediate vicinity of the active site.

Asp70 and Tyr332 residues of peripheral anionic site facilitated the entry of ligands in the active site gorge of enzyme [87]. Residues of the midgorge aromatic recognition region called anionic site (Trp82, Tyr128 and Phe329) actively contributed in binding to quaternary ammonium groups of the incoming ligands via cation-π interactions, thus providing a proper orientation to the compounds inside the gorge. Interactions with aliphatic residues (Leu286 and Pro285) maintained the hollow shape of acyl pocket for stable binding of ligands within the groove of BuChE. Asp197 adjoined to the catalytic triad residue (Ser198) resulted in high electrostatic potential that attracted the tested compounds inside and down the gorge. Cation-π interactions with catalytic His438 near the bottom of the deep gorge were prominently noticed and ligands actively formed π-alkyl contacts with Ala328 in the neighborhood of catalytic Glu325.

3.3.3. Molecular docking study for human NMGAM

All the binding modes for 5a–5j hits were explored using AutoDock Vina. The docked structures exhibited excellent binding energies in the range of −7.5 to −9.1 Kcal/mol. Binding energy scores of all the docked complexes for NMSAM are enlisted in Table 1. Based on docking calculations, the synthesized compounds 5 g, 5i, 5c, 5e and 5d showed better inhibition of human maltase-glucoamylase as compared to standard drug acarbose which is in a good agreement with the results of α-glucosidase assay. 5 g exhibited highest binding energy score of −9.1 Kcal/mol and least IC_{50} value of 1.6Kcal/mol highlighting the significant involvement of specially arranged negatively charged halo groups in interacting with positively charged residues of NMGAM pocket as given in Fig. 4. The synthesized compounds occupied two closely adjacent sites within NMGAM surface as shown in Fig. 3. Accommodation of top ranked potent compounds (5 g and 5c) inside the same groove depicts the importance of basic interacting residues Asn212, His497, Asn498 in establishing contacts with NMGAM. Amino acids spanning the region Asn212- Gly215 were actively interacting key residues in all docked complexes (Table 1). The docking analysis revealed that the van der Waals, electrostatic, and desolvation energies played significant roles in binding. Hydrophobic interactions were mainly donated by Asn212, Leu213, Tyr214, Gly215, Glu446, Leu477, His497 and Asn498 with 6, 9, 7, 9, 5, 5, 6 and 6 compounds, respectively.

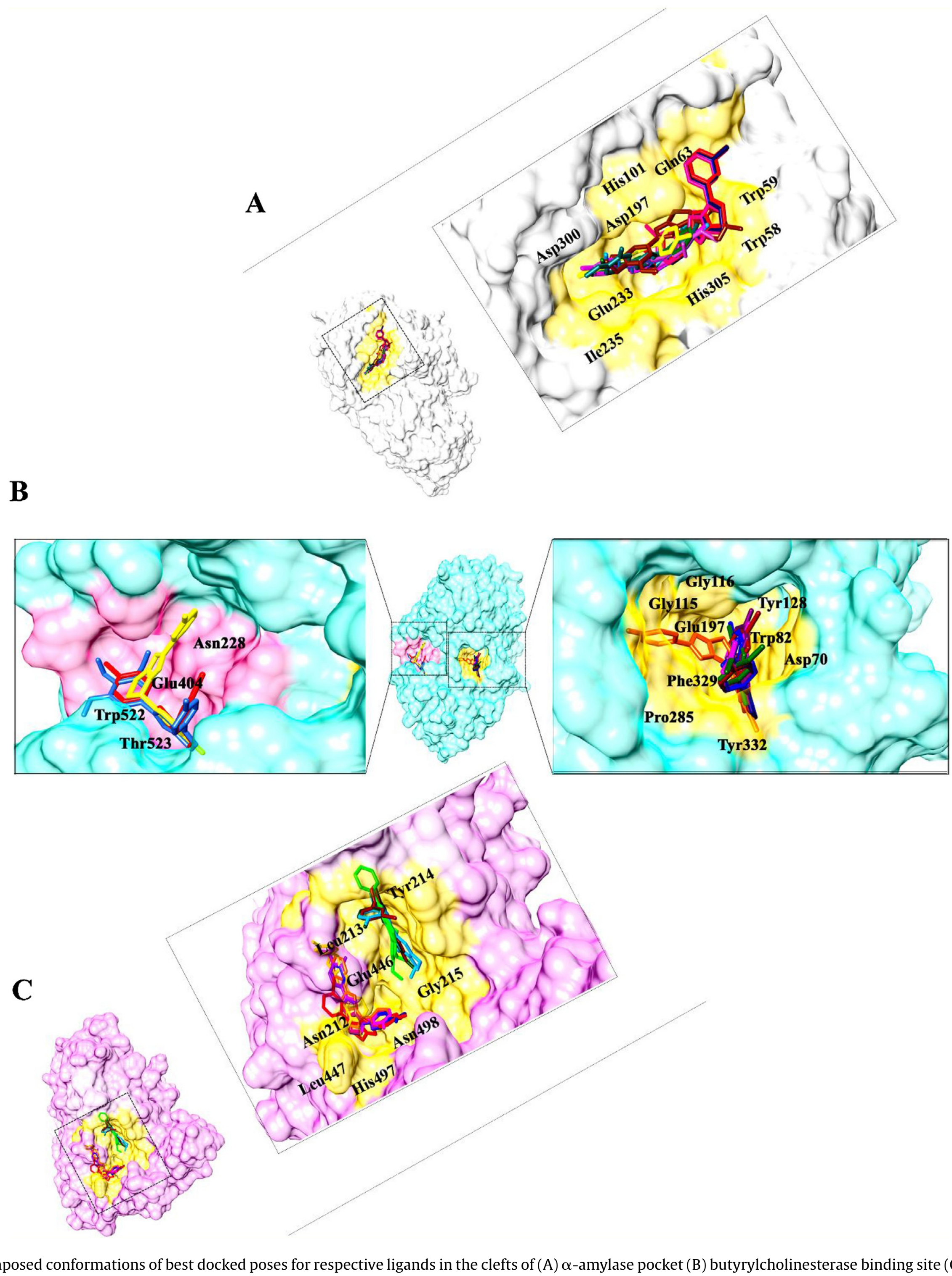

Fig. 3. Superimposed conformations of best docked poses for respective ligands in the clefts of (A) α-amylase pocket (B) butyrylcholinesterase binding site (C) α-glucosidase binding pocket. Binding pocket is indicated by yellow colored surface onto α-amylase, butyrylcholinesterase and maltase-glucoamylase while interacting residues are labelled black. Alterantive binding location in BuChE is colored pink and bound comouunds are indicated by following colors in stick representations: **5a**, Yellow; **5b**, Magenta; **5c**, Dark blue; **5d**, Light blue; **5e**, Orange; **5f**, Purple; **5 g**, Red; **5 h**, Firebrick; **5i**, Dark Green and **5j**, Light green. (For interpretation of the references to colour in this figure legend, the reader is referred to the web version of this article.).

3.4. QSAR modeling

QSAR regression models were developed using most significant descriptors of the compounds as predictive variables. Molecular descriptors screened on the basis of highest correlation with IC_{50} values, along with their physiochemical meanings are given in Table 4. Multiple Linear Regression (MLR) analysis with IC_{50} as dependent variable and selected parameters as independent variables resulted in following optimal QSAR models:

$$\boldsymbol{IC}50(Amylase) = -6.842 + (0.736 * VR3\_Dzs) - (0.884 * VR2\_Dzv) + (345.454 * VE2\_Dzs) + (0.069 * VR2\_Dze) + (14.551 * ETA\_Epsilon\_2) - (17.525 * JGI2) \quad (5)$$

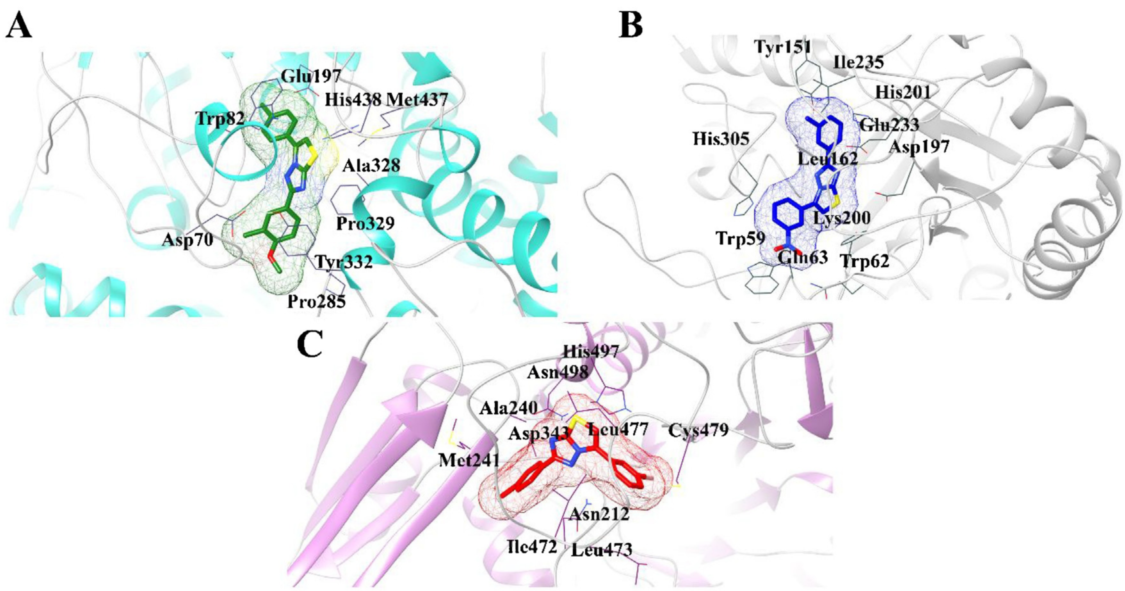

Fig. 4. Detailed interactions of best docked complexes with (A) BuChE, (B) α-amylase and (C) maltase-glucosidase. Proteins are styled in ribbon representations while interacting residues are depicted in wired forms with labelled residues in black color. Bound compounds with minimum IC_{50} value are illustrated in sticks with meshed surface in following colors (**5c**: Dark blue, **5i**: Dark green and **5 g**: Red). (For interpretation of the references to colour in this figure legend, the reader is referred to the web version of this article.).

Table 4
Physical–chemical meanings of the descriptors used in the developed QSAR model.

Descriptors	Chemical Meanings
VR3_Dzs	Logarithmic Randic-like eigenvector-based index from Barysz matrix/weighted by I-state
VR2_Dzv	Normalized Randic-like eigenvector-based index from Barysz matrix/weighted by van der Waals volumes
VE2_Dzs	Average coefficient sum of the last eigenvector from Barysz matrix/weighted by I-state
VR2_Dze	Normalized Randic-like eigenvector-based index from Barysz matrix/weighted by Sanderson electronegativities
ETA_Epsilon_2	A measure of electronegative atom count
JGI2	Mean topological charge index of order 2
ETA_AlphaP	Sum of alpha values of all non-hydrogen vertices of a molecule relative to molecular size
Mse	Mean atomic Sanderson electronegativities (scaled on carbon atom)
Solubility	Aqueous solubility
VE3_Dzv	Logarithmic coefficient sum of the last eigenvector from Barysz matrix/weighted by van der Waals volumes
VR1_Dzi	Randic-like eigenvector-based index from Barysz matrix/weighted by first ionization potential
VE3_Dzi	Logarithmic coefficient sum of the last eigenvector from Barysz matrix/weighted by first ionization potential
SpAbs_Dzs	Graph energy from Barysz matrix/weighted by I-state
Maximum Projection Area	Maximum projection areas of the conformer, based on the van der Waals radius
JGI6	Mean topological charge index of order 6

$$\boldsymbol{IC}50(Butrylcholinesterase) = -192.438 + (85.077 * ETA\_AlphaP) + (150.774 * Mse) - (0.125 * Solubility) \quad (6)$$

$$\boldsymbol{IC}50(Maltase - glucoamylase) = 42.443 + (2.955 * VE3\_Dzv) - (0.053 * VR1\_Dzi) - (0.817 * VE3\_Dzi) - (0.061 * SpAbs\_Dzs) - (0.014 * MaximumProjectionArea) + (205.596 * JGI6) \quad (7)$$

Statistical evaluation of QSAR models included goodness of fit i.e. R^2 (correlation coefficient) and adjusted R^2 (goodness of fit) values as shown in Table 3. The R^2 values of QSAR models were closer to 1 indicating excellent goodness-of-fit while adjusted R^2 values approximating 1 implied robustness of the estimated models. Residual error values depicting differences of R^2 and adjusted R^2 did not exceed 0.3, indicating no over-fitting of predicted models.

QSAR Eq-5 for prediction of IC_{50} value against α-amylase showed that electronic parameters play dominating roles for producing variation in the inhibitory activity. Estimates of the equation suggest that electronegative atoms count, mean topological charge and eigen values from Barysz matrix determine the inhibition potential of a compound where total electronegativity affects positively and mean topological charge correlates negatively with the inhibition activity. The findings suggest the incorporation of further halo groups to increase the net electronegativity and reduce overall topological charge on the molecules for yielding even better IC_{50} values.

Eq-2 proposed negative influence of aqueous solubility on IC_{50} while positive correlation of mean atomic electronegativity and sum of alpha values of non-hydrogen vertices with inhibition activity. The model recommended the incorporation of more strongly electronegative atoms (e.g. fluorine) in the thiazolo[3,2-*b*][1,2,4]triazoles framework for possibly enhancing the inhibitory potential of designed compounds against α-BuChE.

VE3_Dzi and VR1_Dzi are the thermodynamic parameters which depend on first ionization potential of the constituent atoms in the compound. Eq-3 showed their inverse relation with IC_{50} indicating the likelihood inclusion of halo groups having small atomic radius and higher first ionization potentials for improving the inhibition against α-glucosidase. Geometrical and electronic parameters in addition to thermodynamic descriptors also contributed to significant change in the IC_{50} value. The model predicted that greater mean topological charge and reduced van der wall radius/volume may produce the derivative with increased inhibition against NMGAM.

Overall, the findings signify the importance of halo groups in synthesized compounds for governing the inhibitory activity against target proteins in the current study. External validation was performed by predicting IC_{50} values of the compounds through respective QSAR equations and were cross-validated against the known activity values. Observed IC_{50} values of the compounds were in consistency with the predicted values and the data points in the scatter plots showed very less deviation from the normal line (Fig. 5). **5c, 5 g** and **5i** exhibited best observed and estimated IC_{50} values, therefore calculated QSAR models evidently confirmed their potency for inhibiting α-amylase, α-glucosidase and α-BuChE, respectively.

3.5. Pharmacokinetics profiling and toxicity risk analysis

Several physiochemical properties related to pharmacokinetics of synthesized thiazolo[3,2-*b*-1,2,4]triazole derivatives were considered in our study (Tables 5 and 6). The process of excretion, which eliminates the compound from the human body, depends upon its molecular weight. Likewise, low molecular weight is a primary determinant of functional absorption inside the body. All the synthesized compounds weighted less than 500 Da, making them likely to have high solubility and to pass through cell membranes easily (Table 7).

Topological Polar Surface Area (TPSA) is another major factor for determining the rate of molecular absorption and its values for all the compounds lied in normal range (below the cut off 140 Å from as given in Table 4. All the derivatives had polarities that enabled better permeation and absorption, as revealed by lower than 12 cut off value for the sum of H-bond donors and H-bond acceptors (Table 4).

The hydrophilicity and lipophilicity (ratio of a molecule's solubility in octanol to solubility in water) of a compound is measured through logP. High logP value is linked with poor absorption, less blood-brain barrier permeability and increased metabolism in liver while smaller logP values are linked with rapid renal clearance and greater hydrophilicity. Compounds distribution and excretion also depends on logP and for a compound to be well absorbed, its value must not be >5. All compounds in our

Table 5
Statistics of developed QSAR models against target proteins.

Target Proteins	N	R	R^2	Adjusted R^2
Amylase	10	1	1	0.999
Maltase-glucoamylase	10	0.996	0.991	0.981
BuChE	10	0.996	0.992	0.987

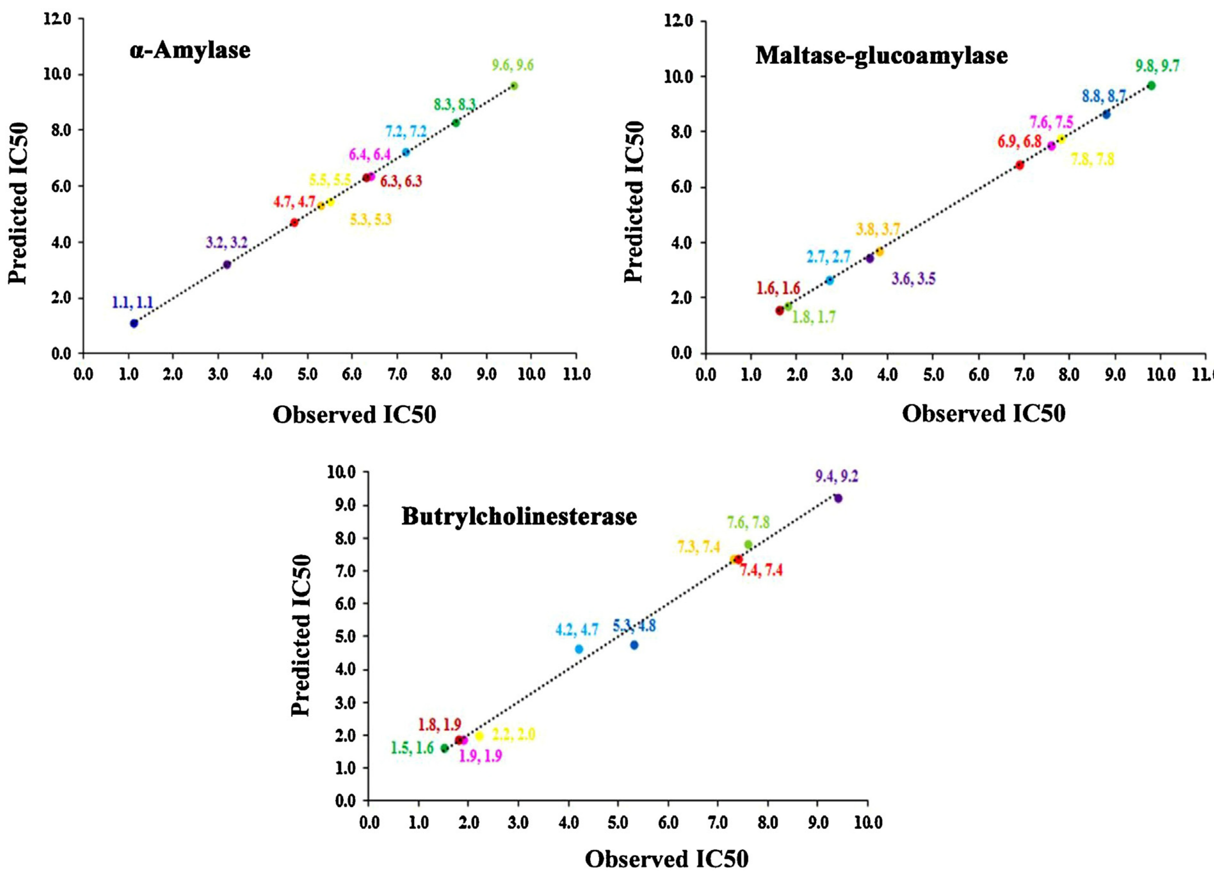

Fig. 5. Statistical cross validation of predicted QSAR models. Experimentally determined IC_{50} values are given on x-axis and predicted IC_{50} values predicted from QSAR equations are on y-axis. Data points and data labels on the graphs are colored according to the types of synthesized compounds (5a, Yellow; 5b, Magenta; 5c, Dark blue; 5d, Light blue; 5e, Orange; 5f, Purple; 5 g, Red; 5 h, Firebrick; 5i, Dark Green and 5j, Light green). (For interpretation of the references to colour in this figure legend, the reader is referred to the web version of this article.).

Table 6
Compliance of the synthesized derivatives with the Standard Intervals for Computational Toxicity Risk and drug-likeness parameters. MUT = Mutagenicity, TUMO = Tumorogenicity, IRRI = Irritation, REP = Reproductive or developmental toxicity, LP=LogP, S=Solubility, DS = Drug score, DL=Druglikeness, MW = molecular weight, HBD = Hydrogen-bond donors, HBA- Hydrogen-bond acceptors and RofV = Rule of five violations.

Compounds	Toxicity Risk Parameters				Drug-likeness Parameters							
	Mut	Tum	Irri	Rep	TPSA	LP	S	DL	MW	HBD	HBA	RofV
5a	No	No	No	Low	56.01	5.57	−6.13	1.1578	396.73	2	3	1
5b	No	No	No	Low	104.25	4.62	4.62	−2.2898	342.42	2	6	0
5c	No	No	No	Low	104.25	4.91	−6.08	−2.2898	338.38	0	6	0
5d	No	No	No	Low	58.43	5.2	−6.21	1.6988	331.8	0	3	1
5e	No	No	No	Low	86.12	4.59	−5.82	2.9457	403.88	0	6	0
5f	No	No	No	Low	58.43	5.37	−6.47	−0.11801	376.25	0	3	1
5g	No	No	No	Low	58.43	5.83	−6.9	1.2488	392.7	0	3	1
5h	No	No	No	Low	58.43	6.25	−7.19	1.1303	386.31	0	3	1
5i	No	No	No	Low	67.66	5.42	−6.18	2.8885	357.86	0	4	0
5j	No	No	No	Low	86.12	3.98	−5.15	2.8993	369.44	0	6	0

Table 7
Pharmacological Activities (pIC_{50}), Ligand Efficiency (LE), Fit Quality (FQ), Partition coefficient (cLogP), Heavy atoms count (HA), Scaled Ligand Efficiency (LES), Lipophilic Efficiency (LipE) Profiles of compounds against α- Amylase, BuChE and Maltase- glucoamylase.

—					**α- Amylase**			A-BuChE			**Maltase- glucoamylase**		
	cLogP	LipE	HA	LES	pIC_{50}	LE	FQ	pIC_{50}	LE	FQ	pIC_{50}	LE	FQ
5a	4.249	4.1227	22	0.69	5.26	2.40	3.52	5.66	2.56	3.72	5.11	2.33	3.4
5b	2.9471	5.5835	24	0.62	5.2	1.19	1.9	5.72	1.30	2.08	5.05	1.15	1.84
5c	2.9471	5.5835	24	0.62	5.95	1.36	2.17	5.28	1.20	1.92	5.6	1.28	2.03
5d	4.2316	4.1419	22	0.69	5.142	2.35	3.42	5.38	2.45	3.57	5.43	2.47	3.59
5e	3.9208	4.4858	27	0.62	5.275	1.20	1.92	5.14	1.17	1.87	5.45	1.23	1.97
5f	4.3508	4.0106	22	0.69	5.494	2.51	3.66	5.03	2.29	3.34	5.16	5.33	7.76
5g	4.856	3.4577	22	0.69	5.327	2.43	3.55	5.13	2.34	3.41	5.92	2.69	3.92
5h	4.9378	3.3687	23	0.69	5.2	2.37	3.45	5.74	2.60	3.8	5.008	2.28	3.32
5i	4.4047	3.9514	24	0.66	5.08	1.74	2.6	5.82	1.99	2.98	5.82	1.99	2.98
5j	3.3148	5.1647	26	0.62	5.017	1.15	1.834	5.11	1.17	1.85	5.11	1.16	1.85

study showed cLogP values less than 5 indicating aqueous solubility and easier access to membrane surfaces (Table 5). In summary, the results revealed that all of the compounds followed Lipinski's rule of five (i.e. Molecular weight: < 500, Octanol-water coefficient (LogP): < 5, H-bond donors: < 5 and H-bond acceptors: < 10).

The plots of cLogP and pIC_{50} showed that inhibition activity gradually improved on increasing the lipophilicity of compounds for α-BuChE while a sharp increasing trend was witnessed with α-amylase (Fig. 6b and c). On contrary, reduction of inhibition potential correlated with higher cLogP values in the case of α-Amylase (Fig. 6a). These findings are exactly in agreement with the fact that 5c with least, 5 g with relatively higher and 5i with highest values of cLogP are good inhibitors of α-amylase, α-BuChE and α-glucosidase, respectively (Fig. 7).

Table 8
Smiles and IC_{50} values of selected compounds from training sets, which were used to predict pharmacophoric features.

	Target Protein	IC_{50}	Smiles
1	α- Amylase	9.28	O=C(N/N=C/CC3=CC=C(Cl)C=C3)C1=CC=C(NC=C2)C2=C1
2	α- Amylase	12.65	O=C(N/N=C/CC3=CC=C(C)C=C3)C1=CC=C(NC=C2)C2=C1
3	α- Amylase	11.08	O=C(N/N=C/CC3=CC=CC(O)=C3)C1=CC=C(NC=C2)C2=C1
4	α- Amylase	9.79	O=C(N/N=C/CC3=CC=CC(F)=C3)C1=CC=C(NC=C2)C2=C1
5	α- Amylase	9.64	O=C(C([H])=C(C3=CC([H])=C(O)C([H])=C3[H])C2)C1=C2C=C(O)C(O)=C1O
6	α- Amylase	4.3	OC1=CC(C3=C(O)C(C2=C(O)C=C(O)C=C2O3)=O)=CC(O)=C1O
7	α- Amylase	4.8	OC1=CC(C3=C(O)C(C2=C(O)C=C(O)C=C2O3)=O)=CC=C1O
8	α- Amylase	5.3	OC1=CC=C(C3=C(O)C(C2=C(O)C=C(O)C=C2O3)=O)C=C1
9	α- Amylase	4.8	[H]C1=C(OC)C(O)=CC(/C=C/C(O)=O)=C1
10	α- Amylase	14	O=C(C([H])([H])C([H])([H])C(C([H])=C1[H])=C([H])C(O[H])=C1O[H])O[H]
11	α- Amylase	5	OC1=C(OC)C=C(/C=C/C(O)=O)C=C1[H]
1	α- Glucosidase	8.48	C=C(N/N=C/CC4=CC=CS4)C(C=C3)=CC=C3C2=NC1=CC=CC=C1S2
2	α- Glucosidase	7.6	OC1=CC(C3=C(OC(O4)C(O)C(O)C4O)C(C2=C(O)C=C(O)C=C2O3)=O)=CC=C1O
3	α- Glucosidase	11.29	O=C(NN=CC4=CC=C(O)C=C4)C(C=C3)=CC=C3C2=NC1=CC=CC=C1S2
4	α- Glucosidase	5.55	O=C(NN=CC4=C(O)C=CC=C4)C(C=C3)=CC=C3C2=NC1=CC=CC=C1S2
5	α- Glucosidase	12.75	O=C(NN=CC4=CC=CO4)C(C=C3)=CC=C3C2=NC1=CC=CC=C1S2
6	α- Glucosidase	5.58	O=C(NN=CC4=C(O)C=C(O)C=C4)C(C=C3)=CC=C3C2=NC1=CC=CC=C1S2
7	α- Glucosidase	8.37	O=C(NN=CC4=C(O)C=C(O)C=C4O)C(C=C3)=CC=C3C2=NC1=CC=CC=C1S2
1	Butrylcholinesterase	4.287	OC1=CC=CC=C1OCC3=NN2C(C4=CC=C(OC)C=C4)=NN=C2S3
2	Butrylcholinesterase	4.987	COC1=CC=C(C2=NN=C3N2N=C(COC4=CC=CC=C4C)S3)C=C1
3	Butrylcholinesterase	1.142	COC4=CC=C(C=C4)OCC2=NN1C(C3=CC=C(OC)C=C3)=NN=C1S2
4	Butrylcholinesterase	3.936	COC1=CC=CC(C2=NN=C3N2N=C(C4=CC=CC(C5=CC=CC=C5)=C4)CS3)=C1
5	Butrylcholinesterase	4.2	ClC1=CC=C(OC(N(C2=CC=CC=C2)C)=O)C(C(C)=O)=C1.ClC(C=C3)=CC=C3NC
6	Butrylcholinesterase	4.3	ClC1=CC=C(OC(N(C2=CC=CC=C2)C)=O)C(C(C)=O)=C1.BrC(C=C3)=CC=C3NC
7	Butrylcholinesterase	1.97	ClC1=CC=C(OC(N(C2=CC=CC=C2)C)=O)C(C(C)=O)=C1.CNC3=CC=C(C(F)(F)F)C=C3

The aqueous solubility(S) of a compound significantly affects its absorption and distribution characteristics and low solubility is associated with poor absorption. The calculated values of the studied compounds were within the acceptable interval (between −6.5 and 0.5 suggested in Table 4. Number of heavy atoms between 20 and 7016, has been proposed to be useful in the prediction of the pharmacokinetic drug-likeness of a compound. All the compounds in our study satisfied this criterion.

We also employed the calculation of ligand efficiency (LE) values for better characterization of the pharmacokinetic behavior of the compounds (Table 5). For thiazolo[3,2-b]-1,2,4-triazole derivatives, smaller ligands such as 5a, 5 g, 5f and 5d exhibited higher efficiency values than the larger ligand. It was also observed that ligands with same heavy atoms numbers (e.g. 5a, 5d, 5 g and 5f) clustered together in the graphs (Fig. 6d, e and f). For the whole data set, it was observed that ligand efficiencies dropped dramatically with the increase of ligand size (Fig. 6). A similar trend has been observed in the literature, with LE showing generally a dependency on ligand size [88].

LipE is a parameter that combines both potency and lipophilicity and is defined as a measure of how efficiently a ligand exploits its lipophilicity to bind to a given target. It has been reported that a lipophilic efficiency greater than 5 combined with clogP values between 2 and 3 is considered optimal for a promising drug candidate [89]. LipE profiles of the compounds 5b, 5c and 5 j identified them as promising candidates as their values reached the standard threshold of 5 (Table 5). However, other compounds also displayed LipE values in acceptable ranges signifying their likely effectiveness (Table 5).

Fit quality score close to 1.0 indicates optimal ligand binding, while low fit quality scores are indicative of suboptimal binding. Use of this criterion showed that all of the compounds under

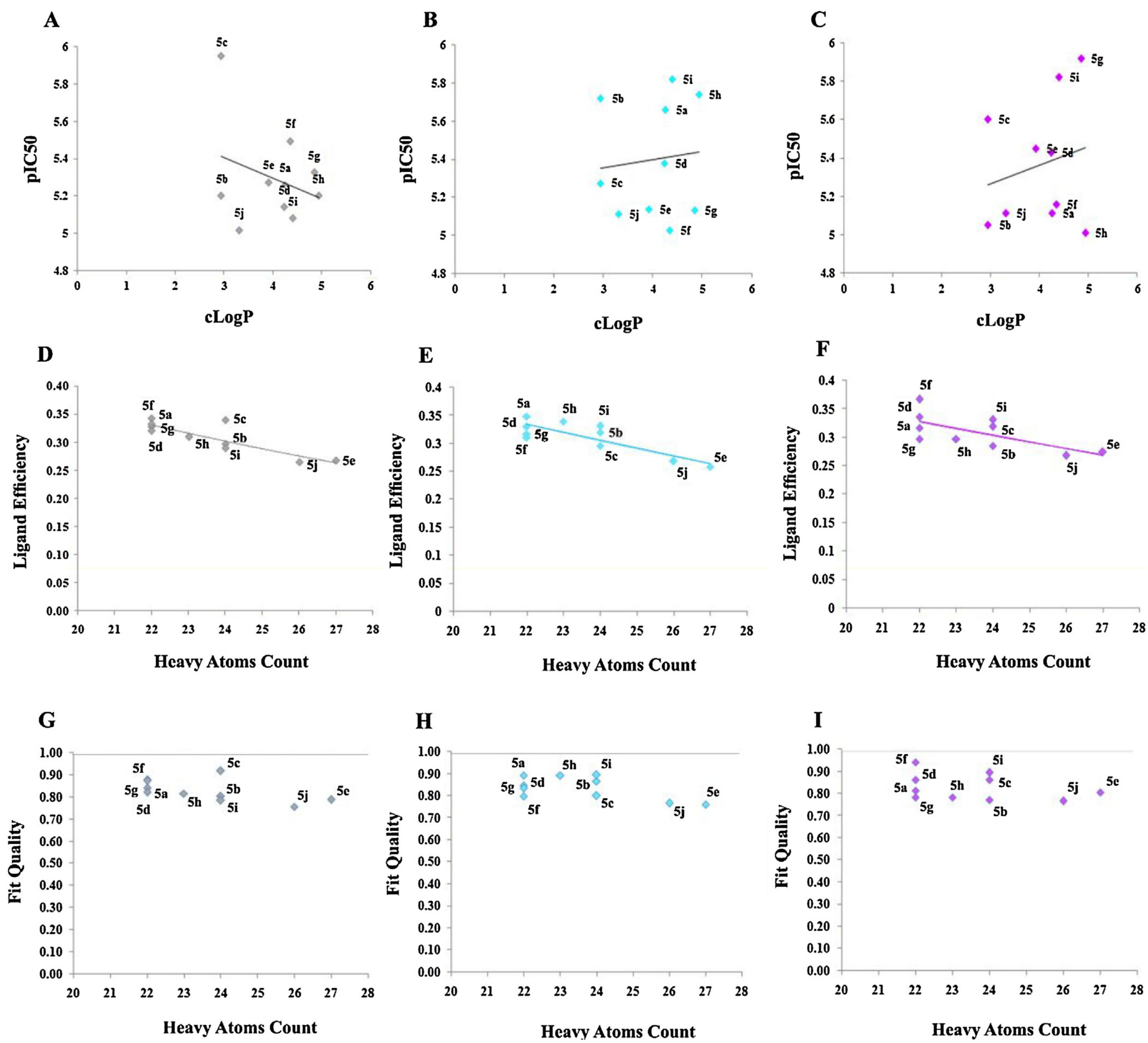

Fig. 6. Correlation of pharmacokinetic properties of the compounds. Colors of data points are represent various target proteins (Grey: α-Amylase, Cyan: BuChE and Magenta: Maltase- glucoamylase). A, B and C) Correlation of inhibitory potency of compounds (expressed as pIC_{50} values) vs cLogP values of the ligands. D, E and F) Plot of ligand efficiency vs heavy atom count for all compounds. G, H and I) Fit quality scores vs heavy atom count. FQ score around 1 indicate a near optimal ligand binding affinity for a given number of heavy atoms.

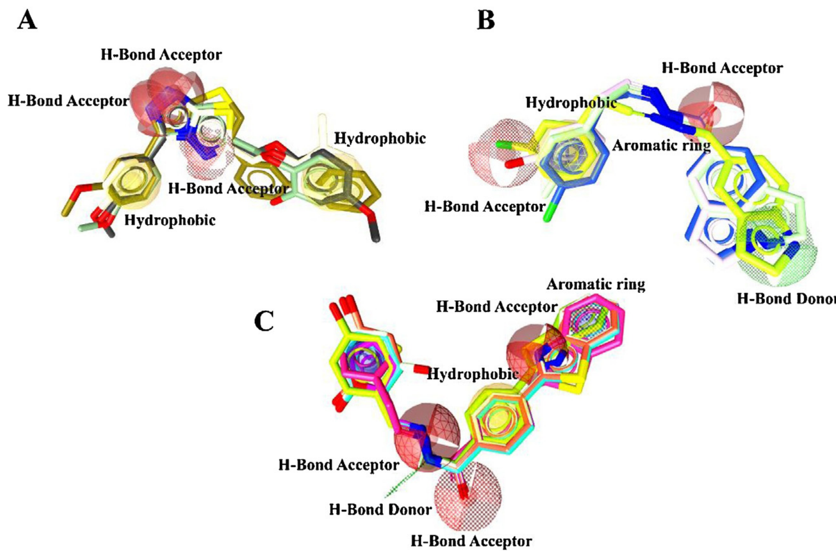

Fig. 7. Pharmacophore feature mapping. Pharmacophoric features of selected inhibitors from training data sets are mapped for Butrylcholinesterase(A), α-Amylase(B) and Glucosidase(C). These features are depicted in green (hydrogen bond donor), pink (hydrogen bond acceptor), cyan (armatic) and golden (hydrophobic) colors. (For interpretation of the references to colour in this figure legend, the reader is referred to the web version of this article.).

present investigation showed FQ scores closer to 1, indicating that synthesized compounds have better in vivo performance based on their ligand binding, potency and lipophilicity profiles (Fig. 6g, h and i).

We predicted toxicity risk parameters for example, mutagenicity, tumorogenicity, irritation and reproductive or developmental toxicities of the synthesized thiazolo[3,2-*b*-1,2,4]triazole derivatives. The toxicity risk predicting softwares locate fragments within a molecule which indicate a potential toxicity risk. Toxicity results from Lazar, Toxicity Checker and ORSIS Data Warrior confirmed that none of the presented compounds has any toxic subcomponent which assures the safety of all compounds for clinical and in-vitro trials.

The training set for QSAR model is included in the Supplementary data. We isolated 50 known thiazol and trizol derivatives for each protein (α-Amylase, α- Glucosidase and Butrylcholinesterase) with IC50 values and listed descriptors. On the basis of descriptor similarity, selected hits were used for pharmacophore generation. The pharmacophore hypothesis with maximized features was tested for 10 compounds (test data set), synthesized in this study. The purpose of 2D QSAR modeling was to elaborate the inhibitory potential of listed hits, as their experimental and predicted IC50 values (through QSAR modeling) are quite similar.

The training data set used in pharmacophore modeling has been listed in Table 7. Predicted pharmacophoric features in inhibitors of α- Amylase, α- Glucosidase and Butrylcholinesterase are represented in Fig. S1 (Table 8).

4. Conclusion

A multistep synthesis of 6-phenyl substituted thiazolo[3,2-b-1,2,4]-triazoles was carried out using $POCl_3$ as an efficient cyclization agent. The newly synthesized compounds were subjected to enzyme inhibition (α-glucosidase, α-amylase and butyrylcholinesterase) essays. All the compounds showed significant potential against these three enzymes. The molecular docking studies were carried out to explore the binding affinity in the target proteins. From the enzyme inhibition studies, we inferred that some derivatives can serve as a template to design potent inhibitors.

Conflict of interest

The authors declare no any conflict of interest

Acknowledgement

We are thankful to Quaid-i-Azam University, Islamabad, Pakistan

Appendix A. Supplementary data

Supplementary data associated with this article can be found, in the online version, at http://dx.doi.org/10.1016/j.biopha.2017.07.139.

References

[1] B.B. Toure, D.G. Hall, Natural product synthesis using multicomponent reaction strategies, Chem. Rev. 109 (2009) 4439–4486.
[2] M.S. Karthikeyan, Synthesis, analgesic, anti-inflammatory and antimicrobial studies of 2, 4-dichloro-5-fluorophenyl containing thiazolotriazoles, Eur. J. Med. Chem. 44 (2009) 827–833.
[3] B.T. Srinivasan, J. Jarvis, K. Khunti, M.J. Davies, Recent advances in the management of type 2 diabetes mellitus: a review, Postgrad. Med. J. 84 (2008) 524–531.
[4] B. Namratha, S.L. Gaonkar, 1, 2, 4-Triazoles: synthetic strategies and pharmacological profiles, Int. J. Pharm. Pharma. Sci. 8 (2014) 73–80.
[5] L.A. Gabriela, F.B. Stefania, G. Bancescu, I. Saramet, G. Saramet, Synthesis and antimicrobial evaluation of some fused heterocyclic [1,2,4]triazolo[3,4- b][1,3,4]thiadiazole derivatives, Eur. J. Med. Chem. 45 (2010) 6139–6146.
[6] T. Taj, R.R. Kamble, A. Dorababu, G.Y. Meti, Synthesis of novel 1,2,4-triazole derivatives as antimicrobial agents via the Japp- Klingemann reaction: investigation of antimicrobial activities, J. Chem. 9 (2013) 706–709.
[7] M. Kumar, S. Yar, B. Srivastava, A.K. Rai, Synthesis, characterization and biological evaluation of novel 1,2,4-triazole derivatives as potent antibacterial and anti-inflammatory agents, Der. Pharma. Chemica. 6 (2014) 137–143.
[8] D. Gupta, D.K. Jain, Synthesis, antifungal and antibacterial activity of novel 1,2,4-triazole derivatives, J. Adv. Pharm. Technol. Res. 6 (2015) 141–146 (Res).
[9] J.N. Sangshetti, R.R. Nagawade, D.B. Shinde, Synthesis of novel 3-(1-(1-substituted piperidin-4-yl)-1H-1,2,3-triazol-4-yl)-1,2,4-oxadiazol-5(4H)-one as antifungal agents, Bioorg. Med. Chem. Lett. 19 (2009) 3564–3567.
[10] J.K. Sahu, S. Swastika Ganguly, A. Kaushik, Synthesis of some novel heterocyclic 1,2,4-triazolo [3,4-b][1,3,4] thiadiazole derivatives as possible antimicrobial agents, J. Appl. Pharm. Sci. 4 (2014) 081–086.
[11] S.G.V. Kumar, D.N. Mishra, Analgesic, anti-inflammatory, and ulcerogenic studies of meloxicam solid dispersion prepared with polyethylene glycol 6000 methods find, Exp. Clin. Pharmacol. 28 (2006) 419–422.

[12] M. Christophe, G. Sylvain, L. Christian, R.P. Maria, F. Frederic, I. Cyril, B. Michel, Synthesis and biological activity of triazole derivatives as inhibitors of InhA and anti tuberculosis agents, Eur. J. Med. Chem. 46 (2011) 5524–5531.
[13] D.R. Godhani, A.A. Jogel, A.M. Sanghani, J.P. Mehta, Synthesis and biological screening of 1,2,4-triazole derivatives, Indian J. Chem. 54 (2015) 556–564.
[14] M. Amir, H. Kumar, S.A. Javed, S.A. Khan, 1,3,4-Oxadiazole/thiadiazole and 1,2,4-triazole derivatives of biphenyl- 4-yloxy acetic acid: synthesis and preliminary evaluation of biological properties, Eur. J. Med. Chem. 43 (2008) 2688–2698.
[15] G.S. Khanage, A. Raju, P. BabanMohite, R. Bhanudas Pandhare, Analgesic activity of some 1,2,4-triazole heterocycles clubbed with pyrazole, tetrazole, isoxazole and pyrimidine, Adv. Pharm. Bull. 3 (2013) 13–18.
[16] D. Sarigol, A. Uzgoren-Baran, B.C. Tel, E.I. Somuncuoglu, I. Kazkayasi, K. Ozadali-Sari, O. Unsal-Tan, G. Okay, M. Ertan, B. Tozkoparan, Novel thiazolo[3, 2-b]-1, 2, 4-triazoles derived from naproxen with analgesic/anti-inflammatory properties: synthesis, biological evaluation and molecular modelling studies, Bioorg. Med. Chem. 15 (2015) 2518–2528.
[17] S.R. Pattan, R.L. Hullolikar, N.S. Dighe, B.N. Ingalagi, M.B. Hole, V.M. Gaware, P. A. Chavan, Synthesis and evaluation of some new phenyl thiazole derivatives for their anti- inflammatory activities, J. Pharm. Sci. Res. 1 (2009) 96–102.
[18] H.M. Ashour, O.G. Shaaban, O.H. Rizk, I.M. El-Ashmawy, Synthesis and biological evaluation of thieno [2′,3′:45] pyrimido [1,2-b][1,2,4] triazines and thieno [2,3-d][1,2,4] triazolo [1,5-a] pyrimidines as anti-inflammatory and analgesic agents, Eur. J. Med. Chem. 62 (2013) 341–351.
[19] R. Romagnoli, P.G. Baraldi, O. Cruz-Lopez, C.L. Cara, M.D. Carrion, A. Brancale, E. Hamel, L. Chen, R. Bortolozzi, G. Basso, G. Viola, Synthesis and antitumor activity of 1, 5-disubstituted 1, 2, 4-triazoles as cis-restricted combretastatin analogues, J. Med. Chem. 53 (2010) 4248–4258.
[20] J.K. Bai, W. Zhao, H.M. Li, Y.J. Tang, Novel biotransformation process of podophyllotoxin to 4b-sulfur-substituted podophyllumderivates with anti-tumor activity by penicillium purogenum, Curr. Med. Chem. 19 (2012) 927–936.
[21] N. Siddiqui, W. Ahsan, Triazole incorporated thiazoles as a new class of anticonvulsants: design: synthesis and in vivo screening, Eur. J. Med. Chem. 45 (2010) 1536–1543.
[22] T. Plech, J.J. Luszczki, M. Wujec, J. Flieger, M. Pizon, Synthesis, characterization and preliminary anticonvulsant evaluation of some 4-alkyl-1,2,4-triazoles, Eur. J. Med. Chem. 60 (2013) 208–215.
[23] V.K. Kamboj, P.K. Verma, A. Dhanda, S. Ranjan, 1,2,4- Triazole derivatives as potential scaffold for anticonvulsant activity, Cent. Nerv. Syst. Agents Med. Chem. 15 (2015) 17–22.
[24] A.K. Jordao, P.P. Afonso, V.F. Ferreira, M.C. De Souza, M.C. Almeida, C.O. Beltrame, D.P. Paiva, S.M. Wardell, J.L. Wardell, E.R. Tiekink, C.R. Damaso, A.C. Cunha, Antiviral evaluation of Namino-1,2,3- triazoles against Cantagalo virus replication in cell culture, Eur. J. Med. Chem. 44 (2009) 3777–3783.
[25] S.h. El-Etrawy, A.A.-H. Abdel-Rahaman, Synthesis and antiviral evaluation of 1, 3-dimethyl-6-(1H-1, 2, 3-triazol-1-yl)pyrimidine- 2, 4(1H, 3H)-dione derivatives, Chem. Heterocycl. Compd. 46 (2010) 1105–1108.
[26] N. Mishra, P. Arora, B. Kumar, L.C. Mishra, A. Bhattacharya, S.K. Awasthi, V.K. Bhasin, Synthesis of novel substituted 1,3-diaryl propenone derivatives and their antimalarial activity in vitro, Eur. J. Med. Chem. 43 (2008) (2008) 1530–1535.
[27] R. Gujjar, A. Marwaha, F. El Mazouni, J. White, K.L. White, S. Creason, D.M. Shackleford, J. Baldwin, W.N. Charman, F.S. Buckner, S. Charman, P.K. Rathod, M.A. Phillips, Identification of a metabolically stable triazolopyrimidine-based dihydroorotate dehydrogenase inhibitor with antimalarial activity in mice, J. Med. Chem. 52 (2009) 1864–1872.
[28] G.V.S. Kumar, Y. Rajendraprasad, B.P. Mallikarjuna, S.M. Chandrashekar, C. Kistayya, Synthesis of some novel 2- substituted-5-[isopropylthiazole] clubbed 1,2, 4-triazole and 1, 3, 4- oxadiazoles as potential antimicrobial and antitubercular agents, Eur. J. Med. Chem. 45 (2010) (2010) 2063–2074.
[29] O. Kouatly, A. Geronikaki, P. Zoumpoulakis, M. Camoutsis Ch Sokovic, A. Ciric, J. Glamoclija, Novel 4-thiazolidinone derivatives as potential antifungal and antibacterial drugs, Bioorg. Med. Chem. 18 (2010) 426–443.
[30] A. Zablotskaya, I. Segal, A. Geronikaki, T. Eremkina, S. Belyakov, M. Petrova, I. Shestakova, L. Zvejniece, V. VizmaNikolajeva, Synthesis physicochemical characterization, cytotoxicity, antimicrobial, anti-inflammatory and psychotropic activity of new N-[1,3-(benzo) thiazol-2-yl]-ω-[3,4-dihydroisoquinolin-2 (1H)-yl] alkanamides, Eur. J. Med Chem 70 (2013) 846–856.
[31] A. Saeed, F.A. Larik, P.A. Channar, H. Mehfooz, M.H. Ashraf, Q. Abbas, M. Hassan, S.Y. Seo, An Expedient Synthesis of N-(1-(5-mercapto-4-((substituted benzylidene) amino)-4H-1, 2, 4-triazol-3-yl) −2-phenylethyl) benzamides as Jack bean Urease inhibitors and free radical scavengers; kinetic mechanism and molecular docking studies, Chem. Biol. Drug Des. (2017), doi:http://dx.doi.org/10.1111/cbdd.12998.
[32] M.S. Mostafa, N.M. Abd El-Salam, Synthesis and biological evaluation of 3-methyl- 2-pyrazolin-5-one derivatives containing thiazole and indole moieties, Der Pharma. Chem. 5 (2013) 1–7.
[33] S.K. Bharti, G. Nath, R. Tilak, S.K. Singh, Synthesis, antibacterial and anti-fungal activities of some novel Schiff bases containing 2, 4-disubstituted thiazole ring, Eur. J. Med. Chem. 45 (2010) 651–660.
[34] N. Sucman, S. Pogrebnoi, A. Barba, A. Geronikaki, O. Radul, F. Macaev, Synthesis and antiviral activity of new thiazole, 1,2,4-triazole and oxindole derivatives, Chem. J. Mold. 6 (2011) 101–109.
[35] A. Geronikaki, P. Vicini, G. Theophilidis, A. Lagunin, V. Poroikov, N. Dabarakis, H. Modarresi, J.C. Dearden, Evaluation the local anaesthetic activity of derivatives of 3-amino-1,2- [d] benzoisothiazoles on sciatic nerve of rat, Eur. J. Med. Chem. 44 (2009) (2009) 473–481.
[36] A. Saeed, P.A. Channar, G. Shabir, F.A. Larik, Green synthesis, characterization and electrochemical behavior of new thiazole based coumarinyl scaffolds, J. Fluoresc. 26 (2016) (2016) 1067–1076.
[37] I. Apostolidis, K. Liaras, A. Geronikaki, D. Hadjipavlou-Litina, A. Gavalas, M. Sokovic, J. Glamoč lija, A. Ciric, Synthesis and biological evaluation of some 5-arylidene-2-(1,3-thiazol-2- ylimino)-1,3-thiazolidin-4-ones as dual anti-inflamatory/antimicrobial agents, Bioorg. Med. Chem. 21 (2013) 532–539.
[38] G. Saravanan, V. Alagarsamy, C.R. Prakash, P.D. Kumar, T.P. Selvam, Synthesis of novel thiazole derivatives as analgesic agents, Asian J. Res. Pharm. Sci. 1 (2011) 134–138.
[39] E. Pitta, E. Crespan, A. Geronikaki, G. Maga, A. Samuele, Novel thiazolidinone derivatives with an uncommon mechanism of inhibition towards HIV-1 Reverse Transcriptase, Lett. Drug. Design. Disc 7 (2010) 228–234.
[40] A. Saeed, P.A. Channar, F.A. Larik, U. Floerke, Facile access to 3, 7-Dialkyltetrahydro-1H, 5H-[1, 2, 4] triazolo [1, 2-a][1, 2, 4] triazole-1, 5-dithiones, Synlett 27 (2016) 1371–1374.
[41] K.D. Hargrave, F.K. Hess, J.T. Oliver, N-(4-Substitutedthiazolyl) oxamic acid derivatives new series of potent, orally active antiallergy agents, J. Med. Chem. 26 (1983) 1158–1163.
[42] B.F. Abdel-Wahab, S.F. Mohamed, A.E.G.E. Amr, M.M. Abdalla, Synthesis and reactions of thiosemicarbazides triazoles, and Schiff bases as antihypertensive a-blocking agents, Monatsh. Chem. 139 (2008) 1083–1090.
[43] V. Gupta, A review on biological activity of imidazole and thiazole moieties and their derivative, Sci. Int. 1 (2013) 253–260.
[44] T. Lino, N. Hashimoto, K. Sasaki, S. Ohyama, R. Yoshimoto, H. Hosaka, T. Hasegawa, M. Chiba, Y. Nagata, J.E.T. Nishimura, Structure activity relationships of 3,5-disubstitutedbenzamides as glucokinase activators with potent in vivo efficacy, Bioorg. Med. Chem. 17 (2009) 3800–3809.
[45] N.D. Amnerkar, K.P. Bhusari, Synthesis of some thiazolyl aminobenzothiazole derivatives as potential antibacterial: antifungal and anthelmintic agents, J. Enzyme. Inhibit. Med. Chem. 26 (2011) 22–28.
[46] Z.Y. Liu, Y.M. Wang, Z.R. Li, J.D. Jiang, D.W. Boykin, Synthesis and anticancer activity of novel 3,4-diarylthiazol-2(3H)- ones (imines), Bioorg. Med. Chem. Lett. 19 (2009) 5661–5664.
[47] E.L. Luzina, A.V. Popov, Synthesis and anticancer activity of N-bis (trifluoromethyl)alkyl-N0-thiazolyl and N-bis(trifluoromethyl) alkyl-N0-benzothiazolylureas, Eur. J. Med. Chem. 44 (2009) 4944–4953.
[48] M.A. Gouda, M.A. Berghot, E.A. Baz, W.S. Hamama, Synthesis, antitumor and antioxidant evaluation of some new thiazole and thiophene derivatives incorporated coumarin moiety, Med. Chem. Res. 21 (2012) 1062–1070.
[49] A.A. Geronikaki, P. Eleni, E.P. Pitta, K.S. Liaras, Thiazoles andthiazolidinones as antioxidants, Cur. Med. Chem. 20 (2013) 4460–4480.
[50] M.V.N. De Souza, M.V. De Almeida, Drogas anti-VIH: passado: presente e futurasperspectivas, Quimica Nov. 26 (2003) 366–373.
[51] F. Rahim, H. Ullah, M.T. Javid, A. Wadood, M. Taha, M. Ashraf, A. Shaukat, M. Junaid, S. Hussain, W. Rehman, R. Mehmood, M. Sajid, M.N. Khan, K.M. Khan, Synthesis, in vitro evaluation and molecular docking studies of thiazole derivatives as new inhibitors of α-glucosidase, Bioorg. Chem. 62 (2015) 15–21.
[52] F. Rahim, K. Ullah, H. Ullah, A. Wadood, A.U. Rehman, M. Imaduddin, A. Ashraf, W. Shaukat, S. Rehman, M. Hussain, K.M. Taha, K.M. Khan, Synthesis molecular docking, acetylcholinesterase and butyrylcholinesterase inhibitory potential of thiazole analogs as new inhibitors for Alzheimer disease, Bioorg. Chem. 58 (2015) 81–87.
[53] G. Tegginamath, R.R. Kamble, P.P. Kattimani, S.B. Margankop, Synthesis of 3-aryl-4-({2-[4-(6-substituted-coumarin-3-yl)-1,3- thiazol-2-yl] hydrazinylidene}methyl/ethyl)-sydnones using silica sulfuric acid and their antidiabetic, DNA cleavage activity, Arab. J. Chem. 9 (2011) 306–312.
[54] M. Balba, N.A. El-Hady, N. Taha, N. Rezki, E.S.H. El Ashry, nhibition of α-glucosidase and α–amylase by diaryl derivatives of imidazole-thione and 1, 2, 4-triazole-thiol, Eur. J. Med. Chem. 46 (2011) (2011) 2596–2601.
[55] B. Fang, C.H. Zhou, X.D. Zhou, Antimicrobial compounds of berberines: research advances, Int. Res. J. Pharm. 37 (2010) 105–109.
[56] D. Genest, C. Rochais, C. Lecoutey, J.S.O. Santos, C. Ballandonne, S. ButtGueulle, R. Legay, M. Since, P. Dallemagne, Design: synthesis and biological evaluation of novel indano- and thiaindano-pyrazoles with potential interest for Alzheimer's disease, Med. Chem. Commun. 4 (2013) 925–9231.
[57] A. Saeed, R. Sajid, P.A. Channar, F.A. Larik, A. Qamar, Hussain Mubashir, U. Raza, U. Flörke, Y.S. Sung, Long chain 1-Acyl-3-arylthioureas as jack bean urease inhibitors, synthesis, kinetic mechanism and molecular docking studies, Journal of the Taiwan Institute of Chemical Engineers 77 (2017) 54–63.
[58] Z. Soyer, S. Parlar, V. Alptuzun, Synthesis and acetylcholinesterase (AChE) inhibitory activity of some N-substituted-5-chloro-2(3H)-benzoxazolone derivatives, Marmara. Pharm. J. 17 (2013) 15–20.
[59] H.A.H. El-Sherif, A.M. Mahmoud, A.A.O. Sarhan, Z.A. Hozien, O.M.A. Habib, One pot synthesis of novel thiazolo [3,2-b][1,2,4] triazoles: a useful synthetic application of the acidified acetic acid method, J. Sulfur. Chem. 27 (2006) 65–85.
[60] R. Pignatello, S. Mazzone, A.M. Panico, G. Mazzone, G. Pennisi, R. Castana, M. Matera, G. Blandino, Synthesis and biological evaluation of thiazolo-triazole derivatives, Eur. J. Med. Chem. 26 (1991) 929–938.

[61] R. Lesyk, O. Vladzimirska, S. Holota, L. Zaprutko, A. Gzella, New 5-substituted thiazolo [3,2-b][1,2,4] triazol-6-ones: synthesis and anticancer evaluation, Eur. J. Med. Chem. 42 (2007) 641–648.
[62] F.A. Larik, A. Saeed, P.A. Channar, H. Ismail, E. Dilshad, B. Mirza, New 1-octanoyl-3-aryl thiourea derivatives: solvent-free synthesis: characterization and multi-target biological activities, Bangladesh. J. Pharmacol 11 (2016) 894–902.
[63] G.M. Morris, R. Huey, W. Lindstrom, M.F. Sanner, R.K. Belew, D.S. Goodsell, A. Olson, AutoDock4 and AutoDockTools4: Automated docking with selective receptor flexibility, J. Comput. Chem. 30 (2009) 2785–2791.
[64] N. Mills, ChemDraw ultra 10.0, J. Am. Chem. Soc. 128 (2006) 13649–13650.
[65] G. Wolber, T. Langer, Ligand Scout: 2005, J. Chem. Info. Model 45 (2005) 160–169.
[66] N.M. O'Boyle, M. Banck, C.A. James, C. Morley, T. Vandermeersch, G.R. Hutchison, Open babel: an open chemical toolbox, J. Chem Informatics 3 (2011) 33.
[67] A.C. Wallace, R.A. Laskowski, J.M. Thornton, LIGPLOT: a program to generate schematic diagrams of protein-ligand interactions, Protein Eng. 8 (1995) 127–134.
[68] N. Arshad, F. Perveen, A. Saeed, P.A. Channar, S.I. Farooqi, F.A. Larik, H. Ismail, B. Mirza, Spectroscopic: molecular docking and structural activity studies of (E)-N′-(substituted benzylidene/methylene) isonicotinohydrazide derivatives for DNA binding and their biological screening, J. Mol. Struct. 1139 (2017) 371–380.
[69] A. Daina, O. Michielin, V. Zoete, Swiss ADME: a free web tool to evaluate pharmacokinetics, drug-likeness and medicinal chemistry friendliness of small molecules, Scientific. Rep 7 (2017) 42717.
[70] M. Cheminformatics, Slovensky grob, Slovak Republic (2013).
[71] C.W. Yap, PaDEL-descriptor: an open source software to calculate molecular descriptors and fingerprints, J. Comput. Chem. 32 (2011) (2011) 1466–1474.
[72] J. Hodgson, ADMET-turning chemicals into drugs, Nat. Biotechnol. 19 (2001) 722–726.
[73] S. Ekins, S. Andreyev, A. Ryabov, E. Kirillov, E.A. Rakhmatulin, S. Sorokina, A. Bugrim, T. Nikolskaya, A combined approach to drug metabolism and toxicity assessment, Drug. Metab. Dispos. 34 (2006) 495–503.
[74] U. Norinder, C.A.S. Bergström, Prediction of ADMET properties, Chem. Med. Chem. 1 (2006) 920–937.
[75] C.A. Lipinski, F. Lombardo, B.W. Dominy, P.J. Feeney, Experimental and computational approaches to estimate solubility and permeability in drug discovery and development settings, Adv. Drug. Deliv. Rev. 46 (2001) 3–26.
[76] R. Kiss, M. Sandor, F.A. Szalai, http://Mcule. com: a public web service for drug discovery, J. Chem. Informatics 4 (2012) 17.
[77] A. Maunz, M. Gütlein, M. Rautenberg, D. Vorgrimmler, D. Gebele, C. Helma, Lazar: a modular predictive toxicology framework, Front. Pharmacol. 4 (2013) 38.
[78] T. Sander, J. Freyss, M. von Korff, C. Rufener, DataWarrior: an open-source program for chemistry aware data visualization and analysis, J. Chem. Inform. Modeling 55 (2015) 460–473.
[79] A.L. Hopkins, G.M. Keserü, P.D. Leeson, D.C. Rees, C.H. Reynolds, The role of ligand efficiency metrics in drug discovery, Nat. Rev. Drug. Discov. 13 (2014) 105–121.
[80] I. Kuntz, K. Chen, K. Sharp, P. Kollman, The maximal affinity of ligands, Proc. Natl. Acad. Sci. 96 (1996) 9997–10002.
[81] P.D. Leeson, B. Springthorpe, The influence of drug-like concepts on decision-making in medicinal chemistry, Nat. Rev. Drug. Disc. 6 (2007) 881–890.
[82] C.H. Reynolds, S.D. Bembenek, B.A. Tounge, 2007: The role of molecular size in ligand efficiency, Bioorg. Med. Chem. Lett. 17 (2007) 4258–4261.
[83] G. Buisson, E. Duee, R. Haser, F. Payan, Three dimensional structure of porcine pancreatic alpha-amylase at 2.9 A resolution. Role of calcium in structure and activity, EMBO J. 6 (1987) 3909.
[84] A. Saeed, P.A. Channar, F.A. Larik, F. Jabeen, U. Muqadar, S. Saeed, U. Flörke, H. Ismail, E. Dilshad, B. Mirza, Design, synthesis, molecular docking studies of organotin-drug derivatives as multi-target agents against antibacterial, antifungal, α-amylase, α-glucosidase and butyrylcholinesterase, Inorganica Chim. Acta 464 (2017) 204–213.
[85] M. Najafian, A. Ebrahim-Habibi, N. Hezareh, P. Yaghmaei, K. Parivar, B. Larijani, Trans-chalcone: a novel small molecule inhibitor of mammalian alpha-amylase, Mol. Bio. Rep. 38 (2011) 1617–1620.
[86] E. Lo Piparo, H. Scheib, N. Frei, G. Williamson, M. Grigorov, C.J. Chou, Flavonoids for controlling starch digestion: structural requirements for inhibiting human α-amylase, J. Med. Chem. 51 (2008) 3555–3561.
[87] D. Sarigol, A. Uzgoren-Baran, B.C. Tel, E.I. Somuncuoglu, I. Kazkayasi, K. sOzadali-Sari, O. Unsal-Tan, G. Okay, M. Ertan, B. Tozkoparan, Novel thiazolo[3, 2-b]-1, 2, 4-triazoles derived from naproxen with analgesic/anti-inflammatory properties: synthesis, biological evaluation and molecular modelling studies, Bioorg. Med. Chem. 15 (2015) 2518–2528.
[88] C.H. Reynolds, S.D. Bembenek, B.A. Tounge, The role of molecular size in ligand efficiency, Bioorg. Med. Chem. Lett. 17 (2007) 4258–4261.
[89] T. Ryckmans, M.P. Edwards, V.A. Horne, A.M. Correia, D.R. Owen, L.R. Thompson, I. Tran, M.F. Tutt, T. Young, Rapid assessment of a novel series of selective CB(2) agonists using parallel synthesis protocols: a lipophilic efficiency (LipE) analysis, Bioorg. Med. Chem. Lett. 19 (2009) 4406–4409.